UNIVERSIDADE D
COIMBRA

Sílvia Sofia da Silva Santos

Robot-based automated disassembly of mobile phone PCB components

Dissertation in the scope of the Master in Physics Engineering supervised by Professor Pedro Mariano Simões Neto and co-supervised by Professor Lino José Forte Marques presented to the Faculty of Science and Technology of the University of Coimbra.

July 2023

Robot-based automated disassembly of mobile phone PCB components

Sílvia Sofia da Silva Santos

A thesis presented for the degree of
Master in Engineering Physics

FACULDADE DE
CIÊNCIAS E TECNOLOGIA
UNIVERSIDADE D
COIMBRA

Faculty of Sciences and Technology (FCTUC)
University of Coimbra
Portugal
July 14, 2023

Supervisor: Professor Pedro Mariano Simões Neto, DEM-UC

Co-Supervisor: Professor Lino José Forte Marques, DEEC-UC

Abstract

Recent studies have shown that electronics contribute to around 50 million tons of waste yearly. In this light, it is becoming increasingly important to focus on developing technologies and processes that are both economically efficient and capable of recovering end-of-life equipment (EOL). Investing in these solutions is crucial for moving towards a sustainable future and seizing new business opportunities. The disassembly stage plays a crucial role in the recovery process of a product. Its efficiency can significantly affect the success of the following process steps. According to recent literature, it has been found that the majority of disassembly work is carried out by hand. The amount of waste electrical and electronic equipment (WEEE) that will need to be recycled and dismantled is expected to grow significantly, which means that manual methods need to be more efficient to handle this increase. As electronic waste continues to increase, there is a greater demand for automated disassembly techniques and plans. The "RECY-SMART - Sustainable approaches for recycling discarded mobile phones" project, which includes this thesis, aims to address this issue. Specifically, it seeks to provide a recycling process focusing on mobile phones, a significant contributor to electronic waste. The process includes all operations, beginning with the initial disassembly task and extending to chemical processes that ultimately sort waste and reusable materials. This study aims to implement a robotic system that automates the disassembly of cell phone printed circuit boards (PCBs) as much as possible. Extensive research was conducted to develop methods for separating components on PCBs while preserving their physical integrity. This involved defining robot paths and manipulation strategies, implementing robotic interaction force control, selecting appropriate desoldering methods, and designing robotic tools. Additive manufacturing was used to fabricate the tools whenever feasible, ensuring the required safety during the procedure. The system underwent testing in an actual real-life situation. The present thesis contains detailed information on various aspects, such as the extraction tool's design, disassembly operation strategy, and manipulation and force control techniques. It also includes a description of the designed extraction tool and the complete strategy for the disassembly operation, covering manipulation and force control. The tool prototypes and force data gathered during the disassembly tests give a complete understanding of the entire process. The transition from desoldering to grasping still poses several challenges and requires further investigation in future studies. Nevertheless, the obtained results are promising and validate the use of the proposed strategy for removing components from cell phone PCBs.

Keywords: Robotics, automated disassembly, electronic waste, PCB disassembly, manipulation, robotic tools.

Resumo

Estudos recentes mostram que os dispositivos de proveniência eletrónica produzem, aproximadamente, 50 milhões de toneladas de resíduos por ano. Neste contexto, torna-se cada vez mais necessário desenvolver tecnologias e processos que sejam economicamente eficientes e capazes de recuperar equipamentos no final da sua vida útil (*EOL*), contribuindo para a criação de um futuro mais sustentável. Dentro das fases associadas aos processos de tratamento de resíduos, a fase de desmontagem desempenha um papel crucial, uma vez que o sucesso da sua execução pode afetar significativamente o desempenho das etapas subsequentes. Segundo literatura recente, a maioria das operações de desmontagem ainda é realizada manualmente, o que se tornará cada vez mais inviável devido ao aumento significativo na quantidade de resíduos elétricos e eletrónicos (*WEEE*) que necessitam de ser reciclados e desmontados. Assim, têm surgido projetos com o objetivo de desenvolver mecanismos que permitam automatizar o processo de desmontagem. O projeto "RECY-SMART - Sustainable approaches for recycling discarded mobile phones", do qual este estudo faz parte, é um desses casos. De forma geral, pretende implementar o processo de reciclagem completo aplicado aos telemóveis, um dos principais contribuintes para o lixo eletrónico. O processo engloba todas as operações, desde a tarefa inicial de desmontagem até aos processos químicos que, por fim, separam os resíduos dos materiais reutilizáveis. A presente tese tem como objetivo implementar um sistema robótico que automatize, na medida do possível, a operação de desmontagem das placas de circuito impresso (*PCB*s) dos telemóveis. Para tal, foi realizada uma investigação intensiva com vista ao desenvolvimento de métodos destinados à extração dos componentes dos *PCB*s, preservando a sua integridade física. O estudo incluiu também a definição de trajetórias e estratégias de manipulação do robô, a utilização de mecanismos de controlo de força, a escolha dos métodos adequados de dessoldagem e o *design* de ferramentas robóticas. Sempre que possível, recorreu-se à manufatura aditiva para a fabricação de ferramentas. Posteriormente, o sistema foi testado em cenários reais. O presente documento apresenta informações detalhadas sobre vários aspetos, como arquitetura da ferramenta de extração e respetivo mecanismo, a estratégia da operação de desmontagem, as técnicas de manipulação e controlo de força. São também apresentados os protótipos da ferramenta e os dados de força recolhidos durante os testes de desmontagem, permitindo uma melhor compreensão de todo o processo. A partir destes resultados, concluiu-se que a transição da fase de dessoldagem para de manipulação ainda apresenta vários desafios e requer investigação adicional em estudos futuros. Todavia, os resultados obtidos são promissores e validam a utilização da estratégia proposta para a remoção dos componentes das *PCB*s dos telemóveis.

Palavras-chave: Robótica, desmontagem automatizada, lixo eletrónico, desmontagem de *PCB*s, manipulação, ferramentas robóticas.

Dedication

This thesis is dedicated to my parents and my sister for being my home and safe place throughout my academic journey. Without your unconditional support, this would not be possible. So, for you, my most resounding thank you.

Declaration

This work is funded by National Funds through the FCT - Fundação para a Ciência e Tecnologia, I.P., under the scope of the project "RECY-SMARTE - Sustainable approaches for recycling and re-use of discarded mobile phones" (PTDC/CTA-AMB/3489/2021) and by the Co-Promotion project "Warehouse of the Future" (reference: IN1167) co-financed by the European Regional Development Fund, through Portugal 2020 (PT2020), by the Competitiveness and Internationalization Operational Programme (COMPETE 2020), and by the Lisbon Regional Operational Program 2014/2020 (LISBOA2020).

Acknowledgements

First, a huge thanks to the project of automatic disassembly process and imaging recognition ("RECY-SMARTE - Sustainable approaches for recycling discarded mobile phones", PTDC/CTA-AMB/3489/2021) for the idea and trust placed to perform the task proposed and to the Co-Promotion project "Warehouse of the Future" (reference: IN1167) by the resources provided for this thesis.

To my supervisor, Professor Pedro Mariano Simões Neto, I have to thank you for all the guidance, concern, example, resources provided, trust, and total availability that was shown to me and to this work throughout these months and that contributed, in a considerable way, to its elaboration and success. To Professor Lino José Forte Marques, thank you for all the human and material resources essential for the execution and success of the proposed task and all pertinent opinions, challenges, and trust given to me during these months. Also, thanks to the researcher Sedat Dogru for his help with the software, experimental tests, and recommendations.

Then, I want to thank all the colleagues of the Collaborative Robotics Laboratory (CoRLuc) for all the help, friendship, opinions, valuable discussions, and meaningful moments. You were indeed a second family, and for that, thank you. To the Embedded Systems Laboratory of the Electrical and Computer Engineering department colleagues, my thanks for sharing knowledge, important discussions, and help.

To all my friends from university and high school, my great thanks for the friendship, sharing, and example of overcoming. To all the teachers who were with me throughout my academic journey, I thank you for the teachings, challenges, wisdom, and management skills I acquired.

To all my family, from my grandparents, aunts, uncles, godparents, cousins, parents, and sister, and boyfriend my most massive thanks for all the support, example, love, and support. You are my daily motivation to work to be and do better.

Finally, I want to thank all the "Grupo de Jovens Mensageiros da Alegria" members for the moments, friendship, and feeling of home. Furthermore, to all the friendships that have emerged this year and have added to my life and the old ones, a special thanks for everything.

Contents

List of Figures

List of Tables

Chapter 1

Introduction

1.1 Motivation

The continuous need for social well-being through technology and its advancement and development have created a global challenge regarding electronic waste (e-waste) treatment [1].

Electronic devices have recently increased due to a fierce competition between technology companies and the constant need to satisfy their customers with new/updated products. That has led not only to some redundancy in the type of technology available but also to a shortening of the life cycle of products [2] and, consequently, to a worrying increase in the waste products they generate [3]. According to recent studies, about 50 million tons of the total annual waste comes from electronics [4]. In 2019, the world population produced almost 53.6 million tons of waste from electrical and electronic equipment (WEEE), and only 17.4% of it passed from recycling processes [5]. Also, in 2030, the figure of 75 million tons of WEEE is expected to be exceeded [6].

In this context, it is essential to increase efforts to develop economically efficient technologies and processes [6] for recovering end-of-life (EOL) equipment in material recycling, product requalification and component reuse [7].

1.1.1 Disassembly

Many authors consider disassembly the first and most crucial step of all the stages of product recovery because the performance of this operation can compromise the success of the next step of the recycling process (Figure 1.1) [2]. An efficient dismantling process can also avoid the excessive use of reagents in chemical processes (leaching processes), which only serve to separate the different metals of interest. Furthermore, it is an alternative process to destructive methods such as crushing, which, although faster, only allows using some recycled materials since it damages the physical integrity of all components [8].

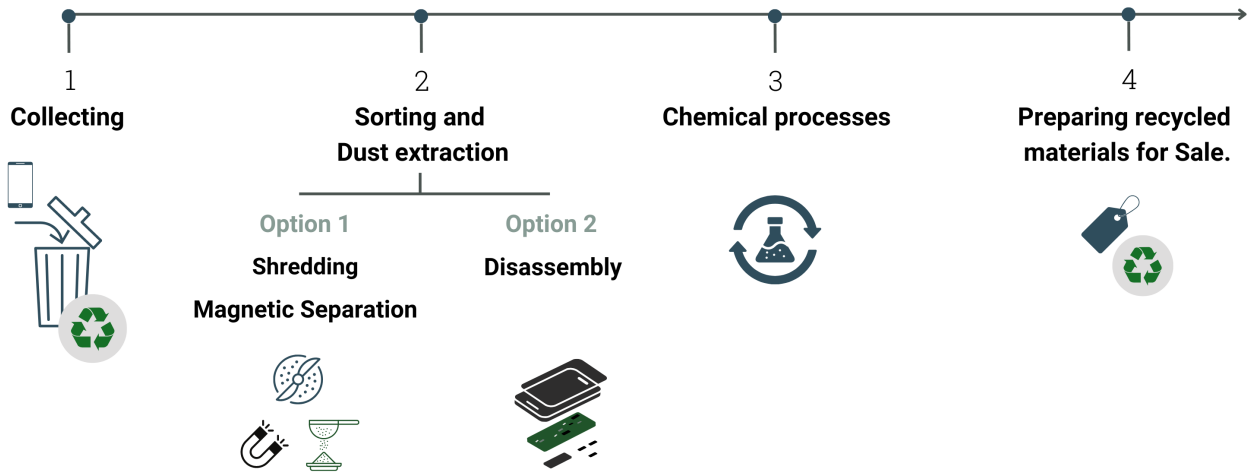

Figure 1.1: Schematic of all phases of an electronic waste recycling process.

Recent literature indicates that most disassembly work is still done manually [7]. This fact is mainly due to the diverse and ambiguous quality and morphology of EOL products, which results in items with very different requirements (for example, handling methods and extraction tools), which implies a high degree of flexibility and adaptability in the disassembly process. However, in the last decade, the number of available workers has decreased and labor costs have increased [9]. Moreover, as the expectation of the number of WEEE to be recycled and dismantled increases dramatically, the manual route becomes less and less efficient [2].

Another important aspect relates to current legislation. In 2003, the European Commission issued a Directive on WEEE, whose main objective was to ensure 70-80 % recovery of this equipment through recovery processes [10]. Regardless, the results have yet to meet expectations. Thus, in the nearest future, stricter legislation is expected requiring all products to be designed to be dismantled in the EOL state. Therefore, developing methods and strategies to automate disassembly is becoming more necessary and relevant. The decline in natural resources needed to produce new equipment and the associated cost also motivate this development.

One of the promising approaches is robotic disassembly since it has a significant advantage associated with the ability to perform repeated tasks [5], resulting in a reduction of operation times and of the total costs associated with the disassembly operation [7]. Furthermore, using methodologies within collaborative robotics will improve work environments [7], contributing to a decrease in the exposure of human operators to toxic substances in materials. The work environment can be shared between the robot and the human operator, fostering cooperation in performing the tasks [11]. However, its implementation still requires further developments, given the assumptions that support the manual route.

1.2 Project description and contributions

The project “RECY SMARTE - Sustainable approaches for recycling discarded mobile phones”, of which this work is part, arises motivated by the previous considerations. It proposes the development and implementation of a complete recycling process applied explicitly to cell phones that include the formulation of all operations, from the initial disassembly task to the chemical processes for a final sorting between waste and materials with interest for reuse. The initial disassembly step expects an automated robotic process capable of extracting some components from the printed circuit boards (PCBs).

The choice of cell phones as the project's target is related to the fact that, like other electronic devices, they have an increasingly shorter life cycle and are quickly seen as outdated by consumers. In addition, their high popularity and constant presence in users' daily lives means they are responsible for much of the current electronic waste [6]. Another aspect is that they present characteristics that result in added challenges, compared to other devices, for implementing an automated disassembly operation. These are their small size, the proximity of the components, and the irregular distribution of the printed circuit boards. Thus, the requirement for separating PCB components contributes to optimizing the entire recycling process. This prior disaggregation will allow the reuse of components that are not damaged (such as integrated circuits, inductors, and connectors) and will optimize the task of extracting the metals of interest (base and precious metals) and critical metals [12], performed until now only in the chemical phase of the process [13] or with magnets or sieves (separation processes [8]) after the primary crushing of the equipment. As such, the proper execution of this task will bring benefits not only from an economic point of view but also from an environmental point of view [14], including the conservation of natural resources and the prevention of unwanted ecological contamination [12]. According to a research group from the University of Sains Malaysia [15], PCBs from cell phones contain about 53.1% base metals (such as iron, copper, aluminum, and nickel), 0.0187% precious metals (such as silver, gold, and palladium), 1.87% critical metals (such as lead). Researchers complete this constitution by stating that the remaining percentage belongs to ceramics and plastics (non-conductive printed circuit board substrates) [16]. Analyzing these data, it may seem insignificant to extract precious metals beforehand due to their tiny percentage. However, when multiplying these quantities by millions of tons, it is expected that the application of the proposed disassembly will avoid using large amounts of chemical reagents, reducing the environmental impact caused by them and saving resources. The fact that PCBs are considered the basis of electric and electronic devices means that the success of the proposed task will contribute to the proliferation of their application in other devices [10].

1.3 Thesis goals

This thesis aims to accomplish the task related to the implementation of a robotic system that allows the disassembly of cell phones' PCBs to be as automated as possible. For that, it is necessary to study technologies and develop strategies to separate the components present on the printed circuit boards without destroying their physical integrity, i.e.:

- Define robot paths and manipulation strategies, including the implementation of robotic interaction force control;
- Choose the correct method for desoldering;
- Design robotic tools that guarantee the safety required during the procedure;
- Fabricate the tools and test the system in a real scenario.

1.4 Outline

The dissertation document has the following chapters:

1. State of the art, to depict what already exists and respective applications in the scope of automated and semi-automated disassembly processes;
2. Methodology, which is a description of the proposed methods for the different stages and their integration.

3. Results and respective discussion, where the main results of the tests performed are presented.
4. Conclusion and future work, that includes an overview of the main results, a description of the problems found and the presentation of solutions to improve the implemented system.

Chapter 2

Literature Review

This chapter starts describes the fundamentals related to the visual servoing control strategy, including applications and calibration procedures, since the input data concerning the position and orientation (pose) of the components in space comes from a vision system. It is essential to note that this study does not address the vision system. However, given its need for integration at a future study stage, it is mentioned and is made a brief review of the associated processes. It also presents the methods associated with robot manipulation and planning, which is common to all structures of this type, regardless of their degrees of freedom and their main inherent issues. Then, the literature associated with path planning that considers the architecture of the surrounding space, which is an essential aspect in dismantling printed circuit boards since it is a limited and small space, is also presented. Removing components from the boards requires contact of the robot with the PCB and its components, making it essential to describe the force and position control mechanisms that ensure the security and success of the process. An analysis of the grippers for grasping and transporting objects with dimensions identical to the PCB components is conducted and a brief review of the processes available for separating the board components. Finally, the general architectures proposed so far for performing robotic disassembly of end-of-life electronic and electrical products are presented. Figure 2.1 illustrates the main steps subject to the study.

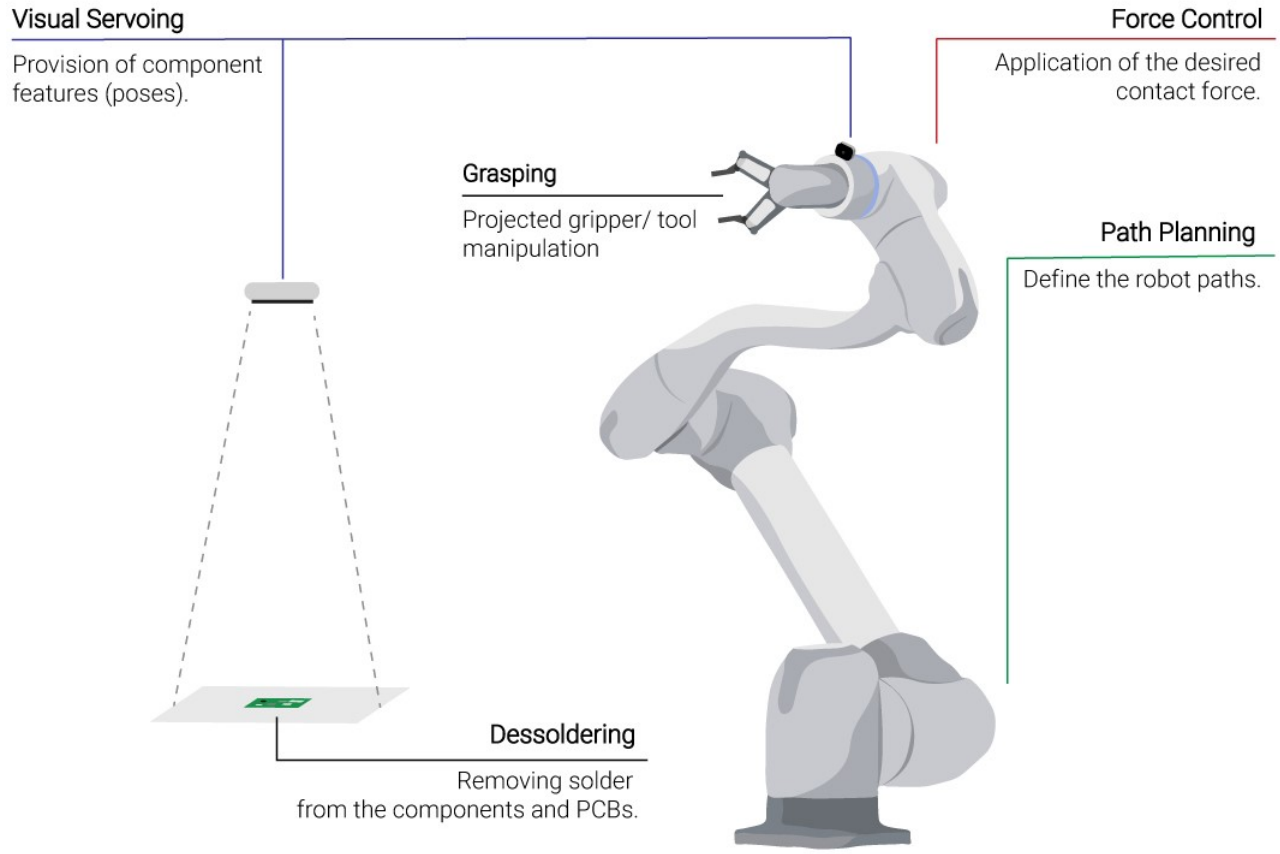

Figure 2.1: Schematic representation of the main research steps under study and the visual servoing step associated with the future vision system integration.

2.1 Visual servoing

The visual servoing technique allows controlling the robot movement (end-effector pose) through data acquired in real-time by the vision sensor using image processing tools, computer vision, machine learning and control [17]. The servoing designation is because of a servo mechanism that uses a feedback system of the relative error of the actual position to the desired one to bring the robot closer to the latter [18].

Through machine learning methods, the system can identify the objects in the environment where it is acting, making the system more autonomous and intelligent since it will act differently depending on the object and not just assume it is an obstacle.

According to the location of the vision system, there are two alternatives [18]. First, the vision system is attached to the robot's end-effector, so its field of view only contains the target in question (Eye in Hand Architecture [19, 20]). In the second one, the camera is near the robot at a fixed position. Hence, the field of view incorporates the end-effector and the target (Eye to Hand Architecture [17, 21]).

Regarding the control procedures, there are two fundamentally different approaches: Position-Based Visual Servo (PBVS) [17, 19, 20, 21] and Image-Based Visual Servo (IBVS) control [22, 23]. In the case of PBVS, it estimates the target's pose using the calibrated vision system. This estimation requires prior knowledge of the target's geometry, the use of the camera's

intrinsic parameters, and the features extracted from the captured image [18, 19]. The calibration values can be obtained using a calibration board (with known points marked on it) and calculating the transformation matrix of its referential concerning the system [19] or using tools from the Robot Operating System (ROS) such as MoveIt [20]. On the other hand, IBVS does not consider the pose estimation step and directly uses the features extracted from the image. Thus, the control is performed only in the image space, and the desired pose is defined implicitly by the image feature values relative to that point [18, 23]. The aim of this type of control is to move the characteristic points of the image to the desired/actual points, which correspond to those of the image taken from the parallel-frontal perspective. The displacement of these points changes the characteristics of the image and, implicitly, the pose of the point of interest. Looking at the two approaches, IBVS brings an added challenge since the features extracted from the image are a highly non-linear function of the camera pose [18, 24]. That is why the applications aimed at implementing the visual servoing technique in a robot in an industrial environment mostly use the PBVS.

2.2 Path planning

In general, path planning is carried out based on robot kinematics [25, 26]. Through this, it is possible to obtain a mapping of the robot's joint angles q, given the end-effector's desired pose (position and orientation). In this way, in situations where the surrounding environment remains unchanged, it is enough to provide the sequence of poses of the robot's end-effector to obtain the mapping of the joints necessary for the movement. However, when the desired action is subject to restrictions over time, it has to take a different procedure to guarantee the operation's success. One of the possible approaches is to look at the method referred to as optimization, which relies on parameters that limit the robot's access to neighboring areas. To do that, first, is defined a nominal position for each joint that is comfortable and safe in the context and, for the case where we have several possibilities of joint angles for the end-effector to reach a specific position, the joint values q are chosen for which the distance between them and the nominal value is a minimum (least squares method). In redundant robots, it is a more complex problem. The great advantage of this procedure lies in the fact that it is possible to solve the problem that takes into account possible restrictions that are associated with the limits of the positions and speed of the joints (even avoiding collisions), many of them described by functions with high non-linearity, through small changes inherent in the nominal position accessible and linear approximations of these constraints. Based on this optimization perspective, it is possible to optimize the entire ideal path by solving a sequence of joint angles, over time, with the same optimization needed for the resolution of an independent scenario. For this, a possible solution is to parameterize the path. This parameterization usually uses more typical functions, such as polynomials. The limits are iteratively redefined using the gradient calculator concerning these parameters and not the values of q [25]. Path planning procedures can also use information from the integrated force, touch, and vision sensors (they provide position and orientation) to serve as parameters for defining the best option for the values of the angles of the joints at that moment.

Most of the recent research focuses on the universe of redundant robots, i.e., they have more than six degrees of freedom (DOF) due to the singularities that they can be subject to. However, this chapter only focuses on strategies highlighted in works directed at non-redundant robots, similar to the one used in this study.

A recent study published in 2022, proposes a strategy based on a random planning scheme in a "tree" structure (Randomly exploring Random Tree algorithms) whose objective is to generate a point-to-point route that satisfies the restrictions of the camera's field of view and the constraints inherent to the space of action [19]. The path obtained contains a series of discrete vectors of the joints (obtained using the Denavit Hartenberg method by defining their coefficients) from q_0 to q_d, where q_0 and q_d are the vectors that contain the coordinates of the joints, q, initial, and final, in shared space. In other words, the robot controller receives information from the vision system, and the vector q chosen is the one that requires the slightest deviation and meets the necessary conditions for the robot to advance to the target, forming a possible 'branch' and constructing the path. In addition, the proposed system admits a speed control to smooth the movement, which takes into account the maximum time allowed for the execution, the restrictions of the speed and acceleration of the joints, and the speed of the tracking sensing system. For future work, the authors consider essential to study the algorithm presented in a dynamic environment, suggesting the introduction of more sensors to obtain information about depth.

A path planning strategy for a robot to pick up screws in its neighborhood for recycling purposes is proposed in [27]. For this, the points associated with the positions of the parts are defined based on the data from the vision system and the use of neural networks (to define the best new point of the path) and of the feasible (collision-free) points in space incorporated into a mesh. In turn, the robot assumed a finite state machine (FSM) with five states:

- Initial state of the robot (home position);
- The state of the accessible nodes adjacent to the analyzed point covered by the robot;
- The state of no accessible nodes adjacent to the analyzed point, not covered by the robot;
- State of the closest node found.
- End state of the process;
- Designated state for the robot when there is an energy or load deficit.

Based on that, an algorithm intends to calculate the next possible node to which the robot should advance by analyzing that point's neighborhood and its state. In this way, the next node is the one where the sum of its position and the cosine of the rotation angle between the current orientation and the direction associated with the next point is maximum.

An essential aspect of path planning, especially in applications such as disassembly, is the implementation of methods that evaluate the best disassembly sequence based on the target geometry and the possible collisions that may occur. In this context, one of the strategies in the literature is using computer-aided design (CAD) software to obtain data regarding the object's geometry and calculate a precedence matrix. This strategy considers the crash test data, which describes all the geometrically feasible disassembly operations for the disassembly of a selected part [28]. Thus, the data regarding the solid's geometric characteristics that allow locating and recognizing them are extracted through a CAD file. These data form the basis of the collision tests, which use the minimum distance between the two parts involved in the action as the threshold value that indicates a possible collision. Thus, through these results, it is possible to constitute a precedence matrix to identify the possible disassembly directions for each component since the columns represent the arbitrary directions evaluated, and each row represents the collision results for a part moving along the directions considered feasible. The number of rows is equal to the number of assembly parts and their level of disassembly. One

strategy to improve the results of the precedence matrices is to introduce an analysis of the propagation of uncertainties associated with geometric parameter tolerances through Monte Carlo methods [29].

2.3 Force control

Robot control is based on the equations of motion inherent in the dynamic model and the principles of control theory. Generally, a robot's link (structure bounded by two consecutive joints) is supported by a reaction force and torque associated with the previous link. In turn, it is subject to its weight and the reaction forces and torques of the links it supports. In addition, the torques of each joint, required for the robot to reach a particular set state, are described by equations of motion (set of coupled dynamic equations) that contain terms relating to inertia, gyroscopic coupling, friction, and gravity [18]. With these equations, it is then possible to obtain a general mapping of the forces associated with the generalized coordinates of the robot joints needed to stabilize the adopted control procedure.

There are two predominant approaches to force control in robotics: passive force and active force control. In passive control, forces are controlled to remain within a specific range of values that guarantee the success of a particular task. The interaction forces modify the path performed by the end-effector, the contact forces are then a residual effect inherent to the action, and there is no measurement of the force being exerted. Implementing this kind of procedure requires a detailed knowledge of all the surrounding space in which the robot will act, implying that all possible obstacles to its movement are appropriately identified. The strategy involves adding flexibility to the final element to cushion impacts and make it more tolerant of eventual positioning errors [30].

On the other hand, in active control, the contact forces are controlled depending on the degree of efficiency required for a given task, so it is necessary to know their value. Thus, the contact forces, in this case, are seen as essential tools for achieving success. In this type of control, the value of the contact forces, known by the force/torque sensors implemented/present in the robot, serves as input to the controller. It is, in turn, used to generate or adapt the path to be performed by the robot to achieve the established goal. For the manipulation of irregular or deformable objects, active control is considered the most appropriate since the applied force factor is a crucial parameter [30].

It is possible to divide active control into two more categories: direct and indirect [30]. Within direct control are the algorithms whose force and position control are performed independently [31]. An example of this type of control is the hybrid position/force control. The basis of hybrid control consists in using the pose information obtained from the direct kinematics equations and the force information from the implemented control circuit, in real-time, as inputs to the robot controller [25] to move the final robot element, in non-deterministic environments, to the desired position [32]. Several modifications have been proposed after this first formulation [33], resulting in new architectures that combine up to the active and passive controls [32, 34].

Regarding indirect control, it aims to control the dynamic relationships between the environment (external forces/torques) and the end-effector by relating the position and force data [31]. The stiffness and damping coefficients are essential parameters in indirect active control [35]. There are two approaches within the latter category: impedance and admittance control. Some researchers interchange impedance and admittance since one is the inverse of the other.

Some researchers even use impedance control in control systems that others call admittance control [30, 31]. Impedance control is based on position control, which requires commands and position measurements to close the feedback loop. It also needs force measurements to realize the desired impedance characteristic. Thus, it uses the different relationships between the acting forces and the robot's position to modify the mechanical impedance of the end-effector to the external forces [36]. In this way, the reference position is transformed into a reference force using an impedance. The most common types of impedance control are stiffness (proportional to position), damping (proportional to velocity), and general impedance (proportional to position, velocity, and acceleration). Analogously, admittance control uses similar mechanisms, transforming the reference force into a reference position using an admittance [31].

To the approaches associated with the indirect active control of force, it is also possible to introduce explicit and implicit designations. Explicit implementations use a force sensor to get the force values from the environment, while implicit implementations calculate those forces through other quantities [31].

Concerning the force and position controllers used in the mentioned architectures, one of the most used controllers for robotic tasks that require control (polishing [37], grinding [38], avoid obstacles/ trajectories [39, 40, 41], assembly [42], disassembly [43]) is the Proportional-Integral-Derivative (PID) controller, and its versions (Proportional-Derivative, PD, and Proportional-Integral, PI), which is based on a closed loop control [44]. In general, the operating principle of a PID controller is described as follows: the controller receives a signal from a sensor, compare it with the desired one (error calculation), and then produces the output signal to the actuator, which is the combination of the proportional, integral, and derivative components calculated over the process. The proportional term only allows generating a system output based on the error calculation of the expected value with the obtained one and a defined gain proportional constant (or matrix of values). The introduction of the proportional term aims to eliminate the residual error by adding a control effect due to the accumulated error value over time. The increase in the integral effect provides a decrease in the proportional effect. As is known from control theory, the integral control action guarantees zero error if the system is stable [45]. However, it brings problems such as potential loss of stability and slow convergence.

Additionally, if the sampling period is slow in force control, the integrator does not eliminate the error. That said, the derivative term is intended to contribute to a better estimate of the future trend of the error of the expected value relative to that obtained based on the current rate of change of the system. Using this term becomes impractical in the presence of sensors that produce significant noise in the system [45, 46]. Therefore, in these cases, the derivative term is eliminated. Due to these considerations, the terms and values used in the controllers should be adapted to each situation.

To carry out robotic processes such as polishing and disassembly, as is the case of the application of this study, it is necessary that the robot has compliance [35, 43]. This property allows the robot to adapt to the surrounding space involving physical contact [31]. The control whose objective is to guarantee the compliance of the robotic system is called compliance control. This control allows deviations from its equilibrium position, depending on the applied external force. The equilibrium position of a compliant actuator is defined as the actuator position where the actuator generates zero force or zero torque. Therefore, by this definition, compliance allows minimizing the impact during the collision of an end-effector with the contacting environment [36]. The categories and architectures presented above for the general force control are applied to this type of control. Active control mechanisms [31, 35, 36], such as position/force hybrid

compliance and impedance/admittance control, are the ones that most contribute to the attribution of greater robot compliance. Although passive control mechanisms are not widely used in applications such as disassembly, they can be more economical when dynamic control is not required [35].

The control of a robot in which the movements are discretized, i.e., forward, back, left, right, up, and down in a straight line, is called Cartesian control. It is useful for applications that just use one of the operations mentioned (polishing and disassembly) since it simplifies the process and avoids problems such as singularities [47, 48].

2.4 Grasping

The grasping action is considered, by many authors, the main component of robotic manipulation intended to control the movement of a given object [49]. Thus, it is crucial to know the primary steps of the procedure and how to plan and evaluate it.

In general, the process of grasping can be described by the following phases [50]:

1. Approaching the object;
2. Coming into contact;
3. Increasing the applied force;
4. Holding/securing action;
5. Moving the object to a target pose;
6. Releasing the object.

Regarding phase 1, the robot uses the surrounding environment data (poses of the elements) from the sensors and the equations used for path planning to place itself near the object of interest. Then, the robot's end-effector contacts the target (phase 2). Within this scope are three possible types of contact described in Table 2.1 [49].

Table 2.1: Description of the possible types of contact during the grasping operation.

Contact Types	Description
Point	It occurs when a single point comes into contact with another point, line (or line segment), or plane. It is considered the most unstable type of contact.
Line	It occurs when a line comes into contact with another line or a plane.The line-plane and non-parallel line-plane contacts are considered stable. However, parallel straight-line contacts are unstable.
Plane	The straight-plane and straight-plane contacts are assumed to be consistently stable. This type of contact can be transformed into point contact by converting a distribution of normal forces along a given region.

In phase 3, a force is applied within limits imposed for the chosen application (according to the morphological and intrinsic characteristics of the object of interest), resulting from the implemented force control system. Phase 4 is considered complete when the required DOF of the object are reduced and, consequently, the applied force stops increasing [50]. This situation can be detected through the information given by the force/torque sensors or by the vision system

through the unchanged variation of the object's geometric center relative to the gripper. At this moment, the object stops moving independently from the gripper. Its movement consists of manipulating the gripper and object system according to a specific path to be followed by the robot. Then, the operation is concluded by releasing the object at the desired location. This action requires a gradual decrease in force and gripper opening or, in the case of vacuum mechanisms, the actuation of an external force that performs component disaggregation. The safety and effectiveness of the entire process are ensured by constantly monitoring the process by the sensors, such as force and torque sensors [50, 51].

Depending on the conditions and complexity of the application, the robotic systems for this type of operation become more challenging and robust. Thus, and due to its importance, several optimizations have been proposed to improve the safety and effectiveness of the entire grasping process. One of the most relevant is the one associated with the object's applied force, which contributes significantly to its equilibrium (without damaging it) and the task's success. In this context, a possible strategy for optimizing the force to be applied is described in [52], whose primary goal is to obtain the set of grasping forces between the gripper and the object of interest that balances its weight and the external forces applied. The selected solution has to minimize the resultant force applied on the object by the gripper contacts (in this case, the gripper 'anthropomorphic hand') and satisfy the constraints of friction, torque, and joint limit. For this, linear and nonlinear methods are used, as well as the formulation of the friction constraints using the linear inequality matrix. The study [52] presents a detailed analysis of the three optimization approaches in the literature, comparing them based on accuracy and computational efficiency. For each method and object of interest, an external force is applied to the target in eighteen different directions to provide a complete picture of the performance of the methods. The performance analysis of the results showed that the nonlinear and linear array approaches perform better in accuracy. In contrast, the computational efficiency of the linear method is more appealing.

2.4.1 Grippers

Considering the purpose of this study, it becomes imperative to know the operating principles and architectures of grippers intended for manipulating objects with identical dimensions as the components of printed circuit boards.

In the literature, for tasks that include the manipulation and picking of objects, the following principles associated with grippers intended for collaborative environments stand out [50, 53]: Mechanical, Suction and Magnetic.

Table 2.2 summarizes the main characteristics of each of the mechanisms, including the principles of actuation and the main models of grippers [50, 54].

Table 2.2: Principles of grasping associated with the manipulation of objects with dimensions identical to those of PCB components and respective descriptions.

Principles	Description
Mechanical	**Principle**: Production of a force between the object and the gripper. **Categories**: Friction and encapsulation of the object's shape. **Operation mode**: Electric, pneumatic, hydraulic and thermal. **Advantages**: Adaptability to different objects, force control to grip the object. **Examples**: Parallel-finger gripper (friction), multiple-finger gripper, gripper with flexible and adaptable material.
Suction	**Principle**: Production of a suction force as a result of activating an airflow in the normal direction to the object in the opposite direction (suction gripper). Application of a high-velocity airflow between the gripper and the object that creates a lifting force due to the pressure difference between the upper and lower objects' faces (Bernoulli gripper). **Operation mode**: Pneumatic. **Advantages**: Lifting of large, flat, and smooth objects, as well as small objects. **Examples**: Suction gripper and Bernoulli gripper.
Magnetic	**Principle**: An electromagnetic force is produced by applying a magnetic or electric field between the gripper and the object. **Advantages**: Lifting metal objects. **Disadvantages**: It can only be used on metallic objects. The final stage of the operation (releasing) becomes complex. **Examples**: Magnetic gripper.

It is possible to improve the gripper performance by integrating a sensor's system into it to ensure greater autonomy and accuracy in the execution of their task [52, 55]. One example is the gripper with a touch sensory system. This solution allows monitoring the grasping, carrying, and releasing of an object by incorporating sensors on the gripper's fingertips. The sensors provide digital force and torque values at high bandwidth and low noise. One of the devices already developed has about 132 tactile pixels with normal pressure sensors and can measure forces up to 100N [50, 52]. However, this configuration can make the solution more expensive.

The strategies related to the release phase of grasping an object can be divided into passive and active categories. In the first case, releasing the object is accomplished by decreasing surface forces, which can be applied within the gripper or at the level of the neighborhood environment (Table 2.3) [50].

Table 2.3: The main passive strategies for performing the release phase of grasping an object.

Field	Description
Gripper	1. Gripper material equal to that of the object to decrease the contact interaction forces. 2. Gripper fingertips with high surface roughness, decreasing the contact area. 3. Hydrophobic coating to prevent moisture absorption.
Environment	1. Dry atmosphere to decrease the effects of surface tension. 2. Vacuum or oxygen-free atmosphere, which reduces the formation of oxides that increase adhesion.

Regarding active strategies, they use an additional force to release the grasped object. Two standard techniques, according to [50, 53], are the use an air pressure generated by compressed air to help loosen the object and the application of inertial forces, such as increased acceleration or vibration of the gripper support.

Although the study proposes a manipulation of the PCB components assuming that the PCBs are already fixed in the working environment, it is important to consider gripper designs that allow proper transport of these boards to the workplace (for an experimental phase of the process). In this context, a group of researchers designed a gripper to transport printed circuit boards of different sizes [56]. Its gripper design is summarized by two parallel fingers made of polyurethane (a polymer widely used in rigid and flexible foams), whose external faces are flat, and the internal ones have a certain inclination to make the gripper adaptable to different types of boards. The tests performed used flexible and rigid polyurethane, and the one that performed better was the gripper made of the latter.

2.5 Desoldering

This subsection briefly describes the main techniques and tools for component and solder separation [57]. Since most of the devices for this purpose are known and have a well-defined working principle, this section discusses it from a practical perspective.

The first technique uses a manual solder sucker, which applies a high-intensity suction force to remove the material. It is considered an appropriate option to selectively remove parts from printed circuit board holes when the solder pins are visible. However, since these instruments are mostly thin and small, they work poorly for tasks that need to remove a large number of components in a short time. Also, it is not a good option for components soldered underneath, as with most cell phone components.

The second procedure used is a solder wick, a copper wire that absorbs solder as the temperature is induced. Unlike the previous process, this option requires extra care in handling as the wick must always be heated to ensure operation.

An alternative to the procedures mentioned above is the one that uses the hot air device. It allows the application of air at a specific temperature (adjustable temperature) associated with the melting point of the solder material on the board or component of interest, removing it. This technique is one of the solutions with more advantages since changing the size of the hot air outlet opening (removable part) makes it possible to choose the action area, giving it versatility.

The fourth technique uses desoldering tweezers that consist of two metal filaments whose temperature is adjusted according to the melting point of the solder. It is a feasible alternative to remove specific components with visible connection pins.

The last technique to be described operates a heated board. This procedure induces a specific temperature, up to the solder melting temperature, in the whole board, allowing simultaneous removal of the components. It is, therefore, the inverse procedure of the second-to-last technique.

2.6 PCB's dismantling systems on frameworks

In [58] it is presented an architecture based on an eye-to-hand approach that uses a robot and a custom robotic tool for the automatic dismantling of larger PCBs when compared to the size of cell phone PCBs. It uses a non-redundant robot, a vision system consisting of an RGB-D sensor and a tool consisting of a sliding axis, a capacitive proximity sensor (which allows the adjustment of the tool on the target), and a programmable screwdriver. The advantage of using this tool is that very high precision in robot positioning is not required. In general, the setup follows the following steps:

1. Processing the acquired image, extracting the component poses;
2. Sending the poses to the robot controller;
3. Activation of the custom tool;
4. Removal of the component of interest by suction.

This architecture, also used in [59], was tested for one type of PCB component (capacitors), so it does not guarantee the reliability of the system for the removal of components with other dimensions and characteristics.

In the automatic dismantling of electronic waste context, such as printed circuit boards from cell phones, the European AIRD study proposes the methodology with the following phases for the disassembly operation [60].

1. Image processing;
2. Robotic manipulation;
3. Use pulsed energy technology for distance measurement, material type identification (laser spectroscopy), and selective cutting of PCB parts;
4. Automatic separation of components into different sorting fractions.

In 2020, the work [61] aimed to implement an automatic disassembly system to recover cell phone central processing units (CPUs) based on a machine vision unit, which means using vision sensors and visual servoing approaches. The proposed architecture for this application contains the mentioned vision system (eye-to-hand), a hot air device to remove the solder, a gripper to transport the CPUs, and a repository for the components. To evaluate the system's performance, cell phones from Apple, Huawei, and Xiaomi were used, so data regarding the temperature required for their disassembly, process time, and the number of tests performed are detailed in the article.

Some studies describe strategies for disassembling electronic equipment without separating the components from the printed circuit boards and defining the best sequence of operations that guarantees the most efficient and adequate disassembly.

In [62] it is presented a strategy for further recovery of strategically essential materials from electric vehicles (down to the PCB board protection capsule) consisting of three main phases:

1. Perform a complete manual non-destructive disassembly to analyze and understand the process, which includes identifying objects of interest and assessing the level of disassembly required.

2. Start an automatic semi-destructive disassembly, having the previous information as a basis, in which is developed the operating environment (robots and tools), design the robotic operations, and test a series of robotic disassembly processes of those mentioned in the literature (including control systems and cutting tools).
3. Validate and optimize the previous step, considering the recovered material of interest. The study describes no specific architecture, only comparing results using different tools and robotic systems.

It is essential to note that in 2019 Apple built a machine to automatically dismantle the cell phone as a whole, in which the components are separated according to their constituent materials [63]. However, there is no separation of the components from the circuit boards without destroying their physical integrity.

To define which is the best sequence of operations, in [64] it is proposed a study of the performance of cutting, unscrewing, and drilling tasks oriented to a given object of interest (in this case, liquid crystal display LCDs), based on geometric models, to implement a more efficient disassembly course of action, i.e., in which it is possible to alternate between the referred operations. After testing various sequences of the operations, the place that each operation occupies in the chosen course of action is associated with the position where it registered the lowest number of failures. The main limitations in this work are related to the need for more detail in the physical models used. Another approach to this topic relates to who performs the tasks inherent to the disassembly process (human operator or robot) to achieve greater efficiency. In this context, some authors agree that there is an advantage when tasks performed manually (human operator), semi-automatically (human operator and robot), and automatically (robot) are combined in a given disassembly process. To prove this, a study published in 2021 performed several steps of a disassembly process using all three methods (where possible) and measured the times required to complete them. After this, the data were compared, and a schedule was created in which each step was assigned the method that guarantees the most efficient process [65]. This procedure was later implemented in 2022, directed at disassembling a hard disk drive, where identical conclusions were obtained [66]. It is important to mention that although the proposal of this dissertation focuses on a fully automated perspective of the process, it is necessary to know other alternatives if the primary factor is execution time.

Chapter 3

Methodology

This chapter describes the methodologies developed based on the state of the art and the conditions under which the system was created. It is divided into the following subsections.

1. Robot and software;
2. Path planning;
3. Force control;
4. Gripper and tool design;
5. Desoldering mechanism;
6. Thermal camera;
7. System integration and architecture.

3.1 Robot and Software

Robot

The robot used in the disassembly cell is the collaborative robot from Doosan Robotics, model M1013 (Figure 3.1). It is a robot with six degrees of freedom and torque sensors in all joints [67]. Although it does not have force sensors in the end-effector, it is possible to access the force values in this region since they are calculated in the robot's controller [68] according to the robot's rigid-body dynamics, using the torque measures values and the kinematics considerations. In other words, the procedure is as the following:

1. It uses the equation of the dynamic (3.1) and the dynamic model and, given the respective vector of generalized joint coordinates q, velocities $\dot{q}$, and accelerations $\ddot{q}$, it computes the torques due to the motion, τ_{dyn} [26].

$$\tau_{dyn} = \mathbf{M}(q)\ddot{q} + \mathbf{C}(q,\dot{q})\dot{q} + \mathbf{F}(\dot{q}) + \mathbf{G}(q) + \mathbf{J}(q)^T f \tag{3.1}$$

   where $\mathbf{M}$ is the joint-space inertia matrix, $\mathbf{C}$ is the Coriolis and centripetal coupling matrix, $\mathbf{F}$ is the friction force, $\mathbf{G}$ is the gravity term, f corresponds to the external force vector applied at the end-effector (force and torque values at the end effector), and $\mathbf{J}$ is the robot Jacobian.

2. It gets the values measured from the torque sensors, τ_s.

3. Using the equation (3.2), it calculates the external torques, τ_{ext}:

$$\tau_{ext} = \tau_s - \tau_{dyn} \tag{3.2}$$

4. At the end, to estimate the external force values, f_{ext}, at the end-effector, the equation (3.3) is computed. The notation $\overline{(.)}$, used in equation (3.3), represents the dynamically consistent inverse of the quantity [69].

$$f_{ext} = \overline{\mathbf{J}}(q)^T \tau_{ext} \tag{3.3}$$

Furthermore, the robot in question presents a maximum uncertainty associated with repeatability of 0.05mm [67], which is acceptable, taking into account the reality of the system to be operated. For example, the minimum distance between components on the PCBs of cell phones is about 0.4mm. The robot has a Teach Pendant that allows the user to visualize and manipulate the values of the generalized coordinates of the joints (joint space) and the pose of the end-effector (task space) in real-time relative to the referential of the Base, Tool, and World. Also, it is possible to implement small algorithms for the execution of simple tasks [70]. Finally, it already brings functionalities that intuitively allow Cartesian and compliance control implementation.

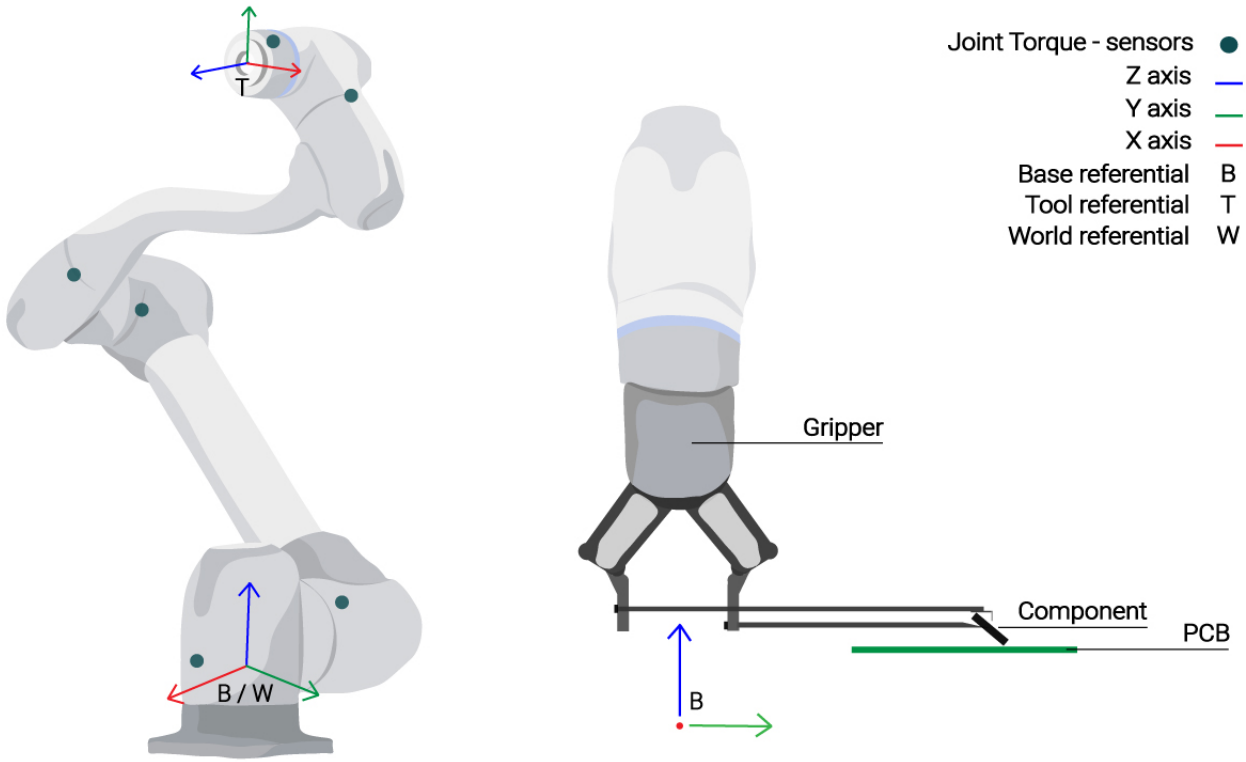

Figure 3.1: Schematic of the Doosan Robotics collaborative robot (model m1013), indicating the respective torque sensors localization and the Base, World and Tool referential, and an overview of the operation to be implemented.

Software

To develop and implement the running algorithms for the dismantling system, a set of software libraries and tools for building robot applications based on ROS were used. This pseudo-operating system has a particular architecture since it is organized into packages. In simple

terms, each package consists of a set of nodes (host operating system process), where each node has a specific functionality. Then, the nodes communicate through topics using a publisher/subscriber mechanism. The node, defined as a publisher, publishes the message (type defined), and the subscriber node reads and uses the information. It is possible for a topic to have more than one publisher and subscriber.

This type of structure allows the algorithm processing to be done in a distributed way, where each package has a function. Also, ROS is an open-source tool that enables the reuse of code (packages, nodes, topics, and messages) already created by other users and the sharing of new code for others to use, which avoids duplicate work, making application development more efficient.

Thus, the choice of using ROS for the development of the project was based on the already mentioned information and the fact that there is a package dedicated to the Doosan robot, allowing the reuse of topics and nodes to implement the system. Regarding simulation environments, the tridimensional robotics simulation system Gazebo and the visualization tool RViz were used. Its use allowed the visualization of paths and debug code functions before moving on to the real mode.

For the design of the extraction tool, the software used was Autodesk Inventor. It allows the CAD design of parts and a simulation of the assembly of all parts.

3.2 Path planning

The path planning was based on the kinematics considerations implemented in the robot controller. Since the robot used is a non-redundant robot and the space of action is not associated with singularity zones (in which it is not possible to relate the pose of the end-effector to the different possibilities of joint variables), it can be deduced that the mapping of the coordinates of the joint velocity space and the operational velocity space is performed based on the equation (3.4) of differential kinematics (direct kinematics):

$$v_e = \mathbf{J}(q)\dot{q} \tag{3.4}$$

where v_e is the vector of end-effector velocity associated with a specific task, $\mathbf{J}$ is the Jacobian matrix, and $\dot{q}$ is the vector of joint velocities. This equation assumes the existence of a linear mapping, although it varies with the current configuration of the robot (due to the presence of the Jacobian element)[71]. Analogously, to solve the inverse kinematics problem, the equation (3.4) becomes:

$$\dot{q} = \mathbf{J}^{-1}(q)v_e \tag{3.5}$$

where $\mathbf{J}^{-1}(q)$ is the Jacobian inverse matrix. In turn, the relationship between the poses and the generalized coordinates of the joints results from the integration of the previous equation (3.5). In discrete time, the integration operation can be computed using numerical techniques (e.g., the Euler integration method).

So, the implemented path can be summarized into five moments:

1. Approach. The pose, relative to the base referential, of the end-effector associated with the side of the component on which the robot operation will be performed (corresponding to the side with fewer components around) is introduced. The data should come from the vision system, but for this first approach, it was placed manually. By inputting the pose of the end-effector through the inverse kinematics, the robot calculates the best solution (there is no unique solution, so it is necessary to define a limit of solutions to be calculated by the system) and moves until there, decreasing the speed value gradually.
2. Contact. In this phase, the robot moves with a linear path along the Cartesian axis on which the desired force to remove the component is exerted.
3. Grasp operation. When the component is gripped, the robot changes its orientation at the level of the robot's joint five (Figure 3.2), increasing the value of this coordinate in joint space.
4. Transport. The robot makes a linear path, relative to the Base, in an upward direction along the height axis to a previously defined height. After this, it makes a linear movement toward the abscissa axis.
5. Release operation. To smooth out the final phase of the process, the robot varies its orientation again at the level of joint five of the robot, decreasing the value of this coordinate in joint space.

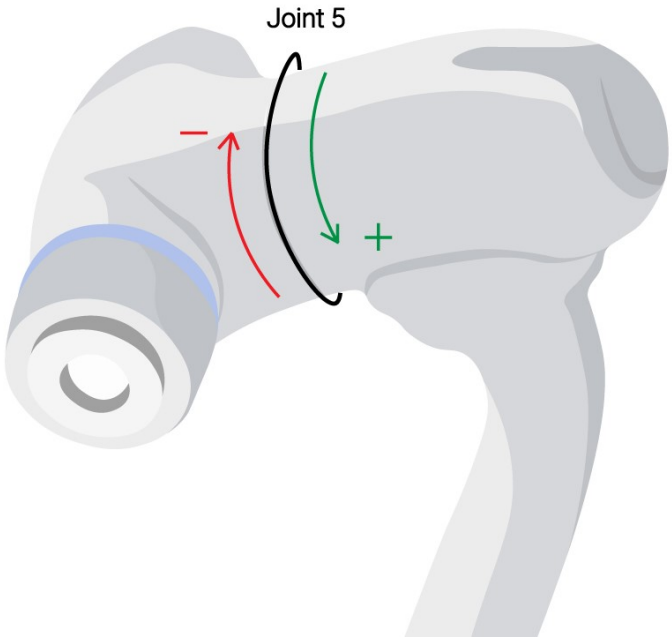

Figure 3.2: Representation of joint 5 and its rotation directions.

Since, in the chosen approach, the robot is acting in a system whose neighborhood is previously known (static environment), there was no need to implement algorithms that would allow the system to deviate from an object/human and recalculate the path.

3.3 Robot control

The robot's interaction control (force and position) was based on the algorithms already integrated into the Doosan M1013 robot associated with the Cartesian active force controls without compliance, in a specific direction, and with compliance, in the remaining directions. The decision to use them was related to the fact that, through them, it was possible to perform the intended action with efficiency and precision (standard deviation presented in the results) adequate to the required application, with no need, for the time being, to implement external control circuits (such as those shown in article [72]) to improve performance. Implementing these may become necessary when introducing the vision system or testing even smaller boards (associated with the new smartphones).

For the Cartesian active force controls without compliance, a function was used to establish a desired value, f_d, for the robot's force in a specific defined direction, according to the extraction direction of the component of interest. In general, the algorithm behind this method uses the data from the force sensors (torque sensors) integrated into the robot (active control) and, by calculating the error, adjusts the current value, bringing it closer to the desired value. It is possible to observe this adjustment in the graphs of the applied force as a function of time, present in the following chapter, especially in the initial phase where an initial overshoot is observed (probably associated with an integral term related to the controller used). It is important to emphasize that the details associated with the function defined in the internal circuit of the robot's controller, that is, the parameters used, such as the gains and matrixes used (for example, stiffness), in the controllers (position and force) and the way the circuit is modeled (mechanisms behind the actuation), depends on the robot. So, all conclusions about its operation are based on its behavior in the system and the possible associations that can be made based on the existing types of control presented in the previous chapter.

A function was used to enable compliance control in the directions in which a specific force value is not applied. That is because, as the distance between the components is minimal, it is expected that the tool developed, at some point, touches other smaller components on the PCB. As such, it is helpful that the robot can make small changes in the path (according to these directions) to adapt and return to the direction established to remove the component. In general, the most commonly implemented compliance control algorithms in this type of robots are the kinematic control algorithms, used to control the position, orientation, and speed of the robot based on sensor information and task commands, and the force control algorithms, which allow the robot to adjust its force or resistance in response to external forces applied during task execution, or a combination of both. It is only guaranteed that the feedback from the sensors is used in the control algorithm for the behavior it admits.

Figure 3.3 shows a schematic of the forces applied to a given component and in a board and the control diagram of the robot [45] (Figure 3.4).

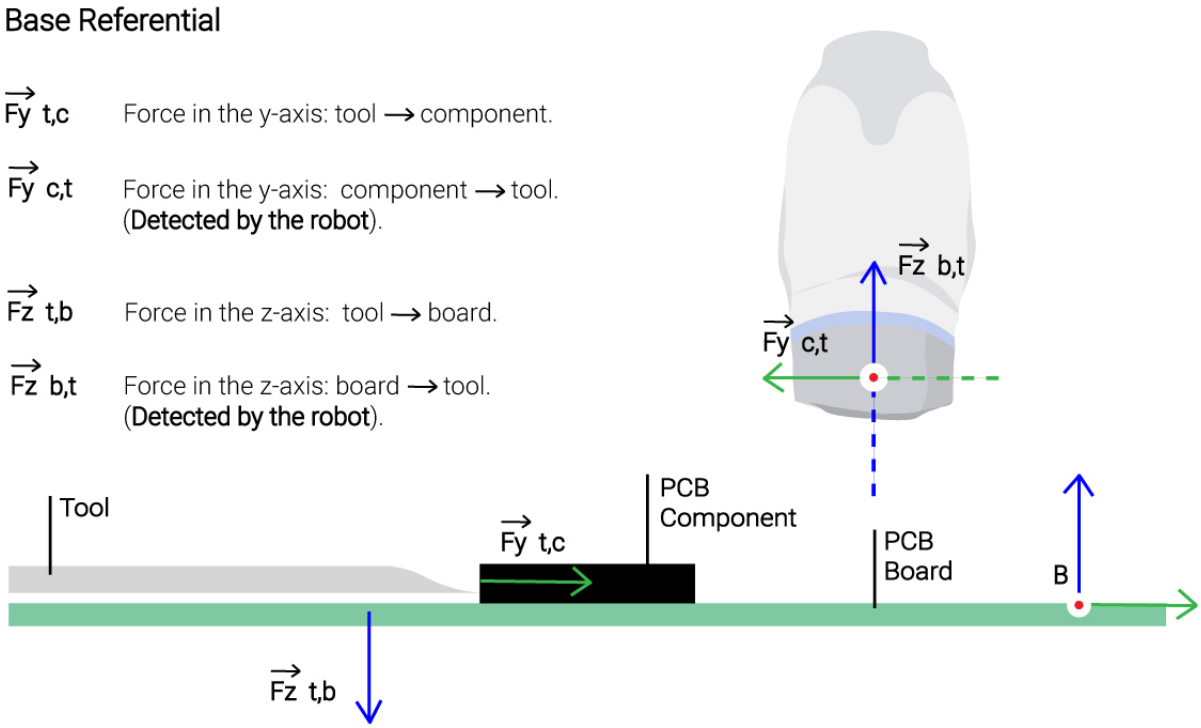

Figure 3.3: Representation of the forces applied, in the contact phase of the tool with the board ($\vec{F_{zt,b}}$) and the component ($\vec{F_{yt,c}}$), and of the forces detected in the robot ($\vec{F_{yc,t}}$, $\vec{F_{zb,t}}$), concerning the referential of the Base.

The contact between the tool and the plate is detected by increasing the force at the z-axis seen at the end-effector, $\vec{F_{zb,t}}$. On the other hand, the solder melting and, consequently, movement of the component is detected by the decrease of the y-axis force, $\vec{F_{yc,t}}$. These conditions are essential for the general algorithm presented in the subsection on system integration.

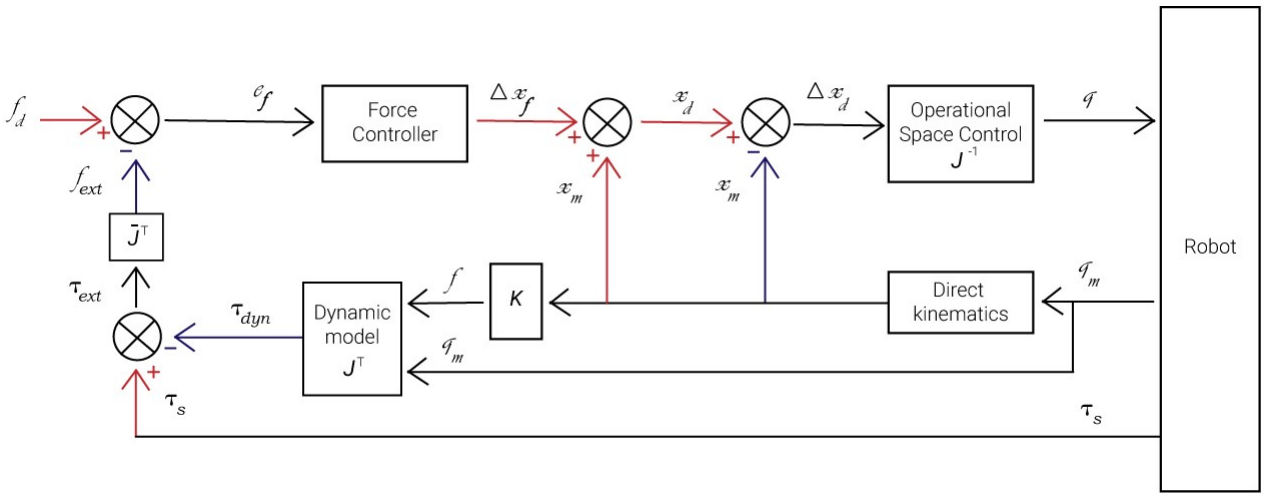

Figure 3.4: Control diagram in the robot controller domain.

In the control diagram presented in Figure 3.4, f_d is the reference force, x_d and x_m are the reference and measured Cartesian position, q_m measured joint coordinates, Δx_f the position displacement and K the stiffness matrix

The operational space block calculates the joint coordinates map through the Cartesian coordinates. Although the force control programming must be in Cartesian space, the control of the motors is in joint space, which makes this transformation necessary.

3.4 Gripper and tool design

3.4.1 Gripper

The gripper available to perform the proposed task is the Onrobot RG6 gripper. It is a two-finger gripper with a removable coating, which allows new materials and tools with different geometries to be adapted. In addition, it contains software features (libraries) that would enable fast implementation, easy customization, and programming (independent of the robot controller). However, it does not have any integrated sensors, which means that all information regarding the system's environment, essential for its integration and control, must come from external sensors (for example, vision sensors) and those integrated into the robot.

Regarding properties such as sensitivity, it has an inadequate sensitivity for the application since the distance between the fingers changes only when an increment of at least 3 millimeters is introduced. This aspect makes it impossible to adjust the finger aperture to the exact size of the components since its sizes (on the boards we had available) vary between 2 and 8 millimeters. Besides that, it also makes it difficult to open and close it smoothly (just achieved with small increments). It is only possible to adjust the grasping force, which affects the speed of the action. To overcome these challenges, a tool was designed, whose description and architecture will be presented next.

3.4.2 Tool

For the development of the tool, the following aspects had to be taken into account:

1. Material. The tool's material had to have a melting point above 300ºC. This characteristic is because it was necessary to subject the components and the whole system to these temperatures. The melting point of the solder, regardless of its material, is not less than 250ºC.

2. Flexibility. The tool had to provide minimal mechanical flexibility to ensure positional stability during the operation.

3. Size/Thickness/Height. That is because the space between the components is minimal, so the tool's thickness to be in contact with the component of interest must also be minimal (thin thickness, about half a millimeter). This characteristic contrasts slightly with flexibility, so the two had to compromise. Also, what connects the tool to the gripper had to be at a height that would not affect the process and would not collide with the components around the one of interest.

4. Contact points. The tool had to come into contact with the component at more than one point to ensure the stability and safety of the grasping process.

5. Mechanism. Its mode of operation would have to be such that the lack of accuracy associated with the gripper opening/close would not affect the process.

The above-designed tool composed of five parts is identified in Figure 3.5.

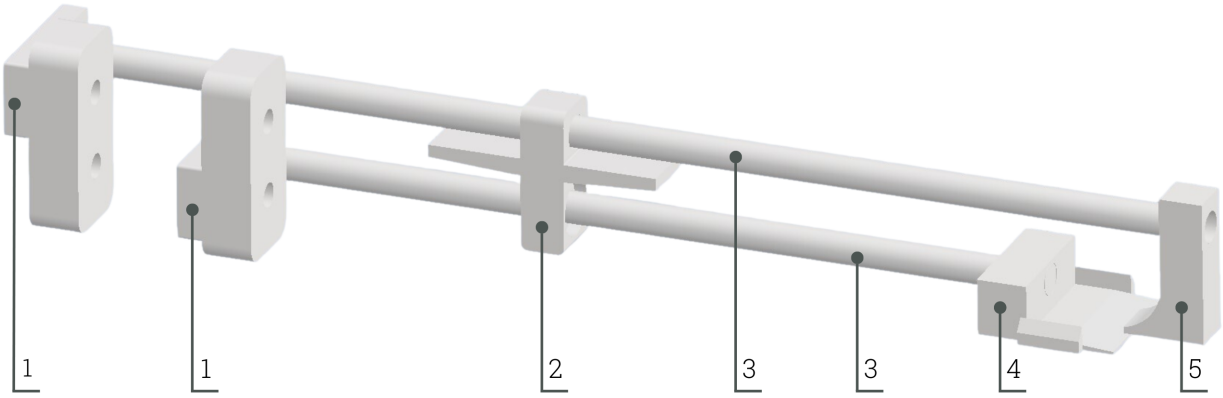

Figure 3.5: Schematic of the designed tool. (1) parts connecting the tool to the gripper fingers, (2) an intermediate part that allows the lower part of the tool to be fixed and the upper part to slide at a defined distance, (3) bars for the support of the whole tool, (4) receiving part that also applies the force in the component to desolder it, (5) and the end part that applies the force to ensure the grasping is performed.

When the gripper is slightly closed, the tool is open, and the opposite is true for the reverse situation. In this way, part 4 of Figure 3.5 comes into contact with the component (plan-line contact) to be extracted and exerts previously defined force in the direction of the tool positioning and part 5 (Figure 3.5). The end part of the tool is thinner to facilitate the ascent of the component from the PCB to the flat part when the solder melts. In addition, it has a slight tilt to ensure that the components behind it do not interfere with the operation (the angle was set to the maximum height of the components). The two sidebands help the component stay where it is supposed to and help to reduce the flexibility of this part of the tool (U-shaped geometry). Regarding part 5 (Figure 3.5), it is responsible for facilitating the process of lifting the component to be extracted and for holding the component after it is at part 4 (Figure 3.5). In the grasping situation, the fingers raise their height slightly, which makes part 5 (Figure 3.5) rise above the piece, holding it. This mechanism allows a large part of the process to be carried out by part 5 (Figure 3.5), and part 4 (Figure 3.5) only has the function of holding, i.e., the distance between them does not need to be precisely the size of the PCB component. In the last phase of the process, it is even advantageous that the distance acquired between the tool's two parts is smaller than the component size.

Part 2 (Figure 3.5) is an intermediate component that causes the bottom part of the tool to be fixed and the top part to slide over it. Also, it maintains the distance (equal to the distance between the gripper's finger screws). It ensures stability and more stiffness associated with the structure composed of part 3 shown in Figure 3.5.

Concerning the material in which the tool was made, all parts were made of galvanized steel (melting point above 1000ºC), except for parts 1 and 2 (Figure 3.5), which were made of Polylactic acid (PLA) and fabricated using additive manufacturing, since they at a considerable distance from the heating source. For part 4 (Figure 3.5), different prototypes, shown in chapter Results and Discussion, were projected in which the contact area and the geometry of the end part were changed. The tool's mechanism is identical to a push-pull system, illustrated in Figure 3.6.

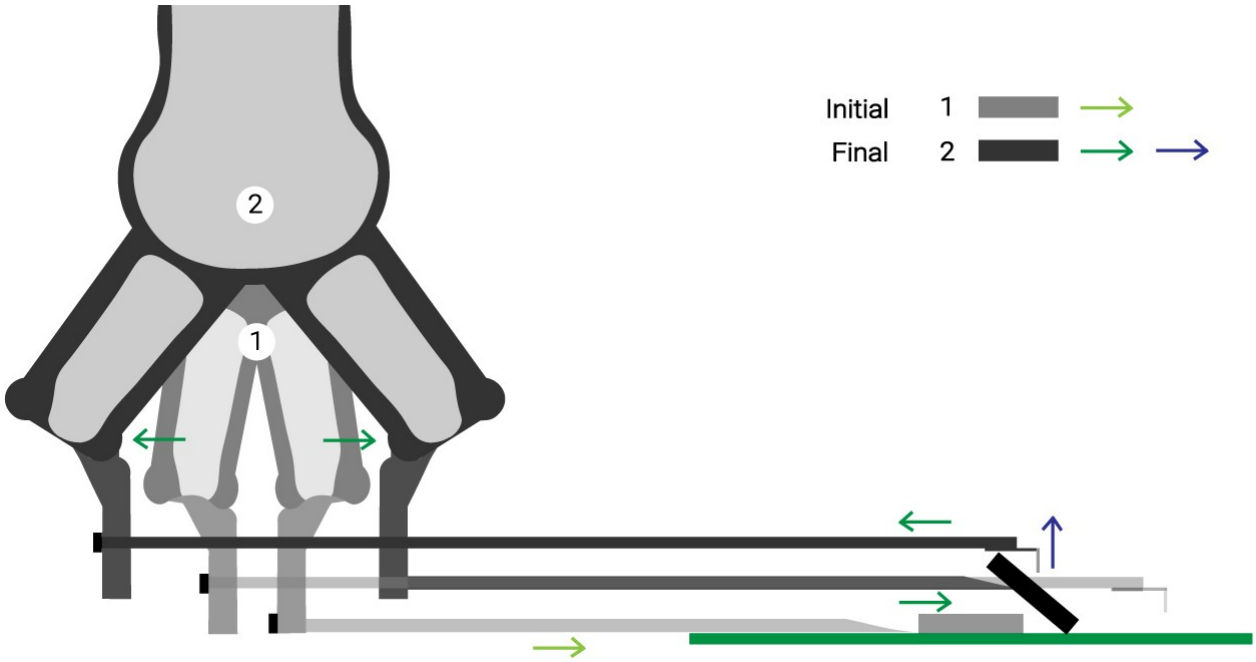

Figure 3.6: Schematic of the push-pull mechanism of the developed tool.

3.5 Desoldering mechanism

For the desolder phase, a hot air device and a heated plate were used. The choice of the first device was related to the fact that its temperature can be adjustable and that it allows the direct application of heat in a specific region of interest, which is essential for the execution of the extraction task. Thus, to improve the mechanism implemented, information was collected (techniques in Table 3.1, crucial factors in Table 3.2 and strategies in Table 3.3) about techniques that facilitate the process, the key factors that affect it, and possible strategies to apply in the procedure.

Table 3.1: Techniques to improve the hot air desoldering mechanism.

Techniques		
Material	**Application Procedure**	**Function**
Flux	Apply to solder connections or component borders with non-visible connections.	1. Remove metallic oxides from solder connections. 2. Aids heat transfer by increasing the fluidity of the solder.
Lead Solder	Apply a low quantity to lead-free connections.	Decrease the melting point of the mixture.

Table 3.2: Key Factors that affect the hot air desoldering mechanism.

Key factors	
Parameter	**Description**
Solder material	It influences the melting point. The higher this value is, the higher the heat the components are subjected to.
Component mass	It affects, generally, the number of connections and, consequently, the exposure time to heat. A more significant number of connections implies a longer exposure time.
PCB's Layers	One of the most present elements in boards' layers is cooper, which is a good conductor. A higher number of layers implies more quantity of this element and, consequently, more heat dissipation. Thus, a longer exposure time is required.
Application distance	It affects the heat stress felt at a single point of the board. It is advisable to apply the heat source from a larger distance or to make a continuous movement (circular or linear) to reduce the stress at a single point.

Table 3.3: Strategies to apply in the hot air desoldering procedure.

Strategies in Procedure	
Phase	**Description**
Heat application	Sometimes it is not straightforward to define the correct temperature to apply. When the components outside the rework area start to melt or the opposite side of the board gets too hot, it indicates that the temperature is too high.
Remove components	The components should be removed immediately as soon as they come loose.

The heat source application was made manually. One robot intended for the manipulation part was used. Based on that, regarding the techniques presented in Table 3.1, only the flux was used since lead solder would harm the operator's health.

Introducing the heated plate, where the PCBs were placed, into the system decreased the chance that components would instantly reattach to the plate after desoldering. In addition, keeping the plate at a temperature slightly below the melting point of the solder contributes to its generalized heating, making it easier to remove components, particularly after the first extraction.

3.6 Thermal camera

To improve and optimize the disassembly process, a thermal camera was introduced to the work cell. The camera is the FLIR Lepton (LWIR Micro Thermal Camera Module, model Lepton 2.5). This thermal camera has 80x60 active pixels and can provide accurate and calibrated temperature data associated with each pixel. In general, the working principle of this type of camera is based on the detection of infrared energy from objects (heat) and its subsequent conversion into a digital image. Furthermore, a FLIR camera like the one used can detect slight differences in heat - as small as 0.01°C - and display them as shades of gray, Figure 3.7 (a), or with different color palettes.

The introduction of this device in the system implied the development of a node in ROS intended to read the temperature values and of a topic where these values are published and, subsequently, read by the control node of the robot (used in the integration algorithm and system control). Since there is no hotter element within the defined region of interest than the plate on which temperatures above 300ºC are falling, only the maximum temperature value is published to simplify the conditions used in the algorithm. However, it is possible to access the data for the entire region whenever necessary. In addition, each time the camera node runs, a real-time image is displayed in grayscale, where the maximum and minimum temperature points are marked. This image allows the user to get an idea, through visual analysis, of the behavior and thermal state of the system.

The data from the camera allowed us to define the range of system temperature values associated with the phase in which the plate is significantly hot and still below the melting point of the solder (approximately 100ºC), i.e., when hot air can be applied. It was also possible to define the range of system temperature values (there is always a specific variability associated with the type of plate, amount, and material of the weld) relative to the situation where the temperature is close to the melting point (above 220ºC), which indicates that the tool can approach and start applying the force. These values were defined based on the observed values, indicative of the mentioned stages, in the different tests performed (five different PCBs). Thus, using this device made it possible to decrease the exposure time of the tool to high temperatures and thus save energy resources.

Regarding the camera's support, it was designed to take advantage of the four holes that are part of the PCB that contains it, to fix it, and to allow the cable to pass through. Besides that, since it was set at a height of 80cm, the support was manufactured using additive manufacturing (Figure 3.7 (b)).

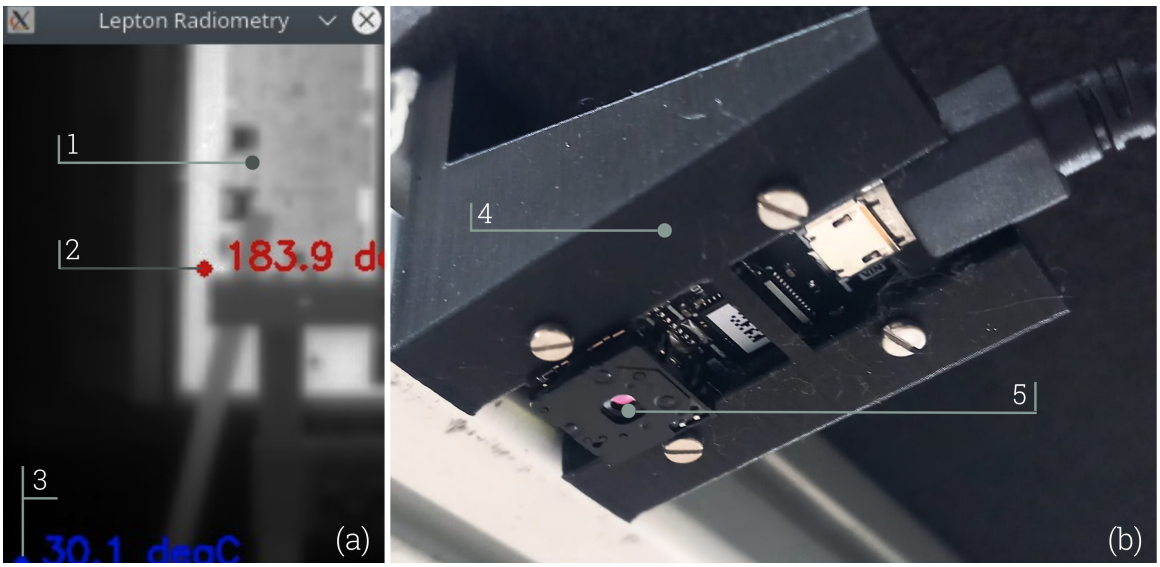

Figure 3.7: Thermal camera. (a) Example of a digital image from the thermal camera in grayscale. (1) PCB, (2) Pixel with maximum temperature, and (3) Pixel with minimum temperature. (b) Image of the (4) support and (5) FLIR Lepton camera.

3.7 System integration and architecture

This section describes how the whole system was integrated. Firstly, the hardware connections are presented. Secondly, the flow diagrams with the implemented algorithm are detailed. Finally, the ROS map demonstrates the integration of the nodes and topics used and the type of messages exchanged.

3.7.1 Hardware connections

The hardware connections of the whole system are detailed in Figure 3.8.

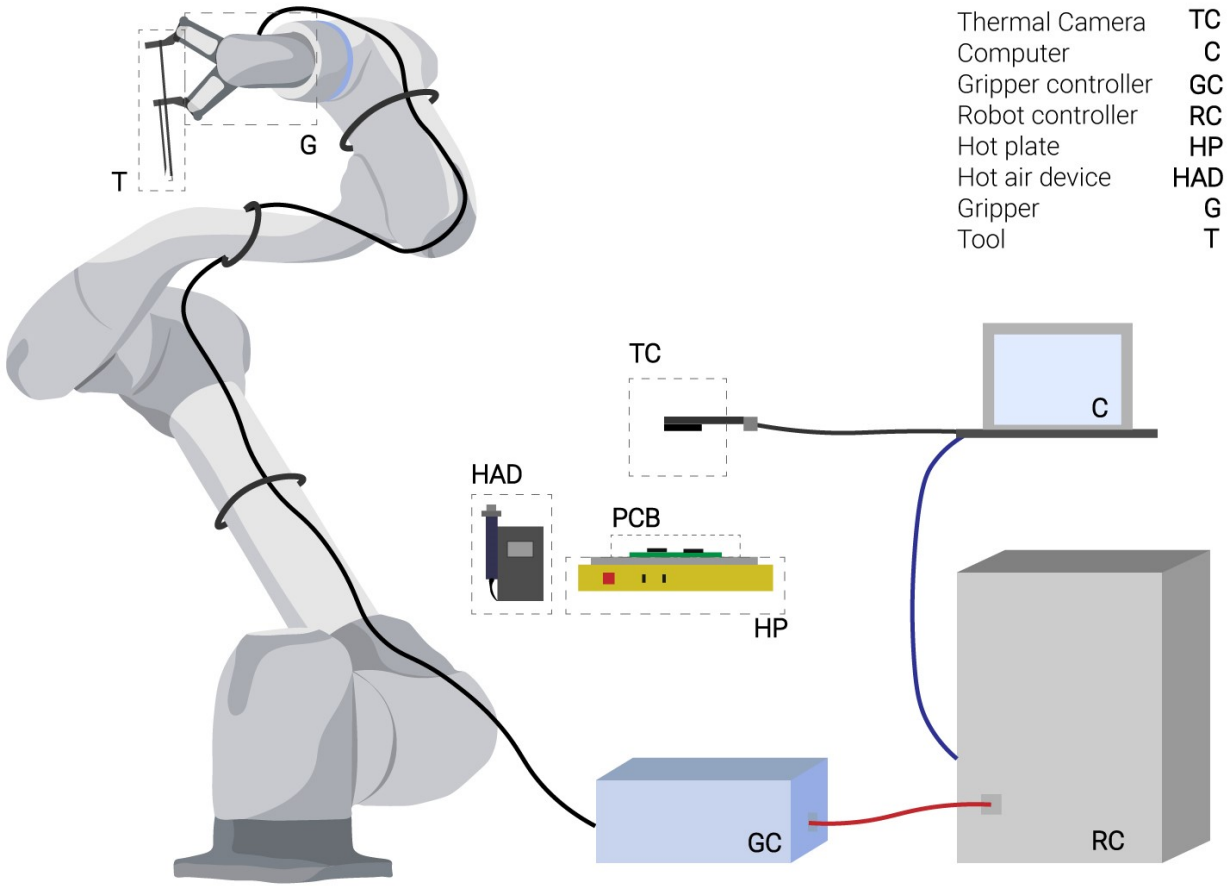

Figure 3.8: Hardware connections.

As Figure 3.8 represents, the gripper has its controller connected to the robot controller using I/O. This aspect conducted the integration between its controller and the robot controller to become possible to control both with the same computer system. Then, the connection of the gripper controller using an Ethernet communication cable. The thermal camera described in subsection 3.6 is connected to the computer by a USB serial cable.

3.7.2 Disassembly strategy

The purpose of this subsection is to present and describe, in a schematic way (through flow charts), the algorithm's structure developed for the execution of the entire disassembly operation. It should be noted that aspects such as the temperature values used in the conditions on which critical stages of the process depend (for example, when the robot can approach the

component) have already been discussed throughout the chapter. Therefore, they will not be explored here.

Another important factor is related to the thermal camera. Although it allows data access (display of a setup image with temperature data), in real-time, throughout the whole process, the values provided by it only intervene in the algorithm in the phase before and in the decision-making for the beginning of the contact phase of the tool with the PCB component of interest. Thus, the algorithm diagram associated with this is presented separately in Figure 3.9.

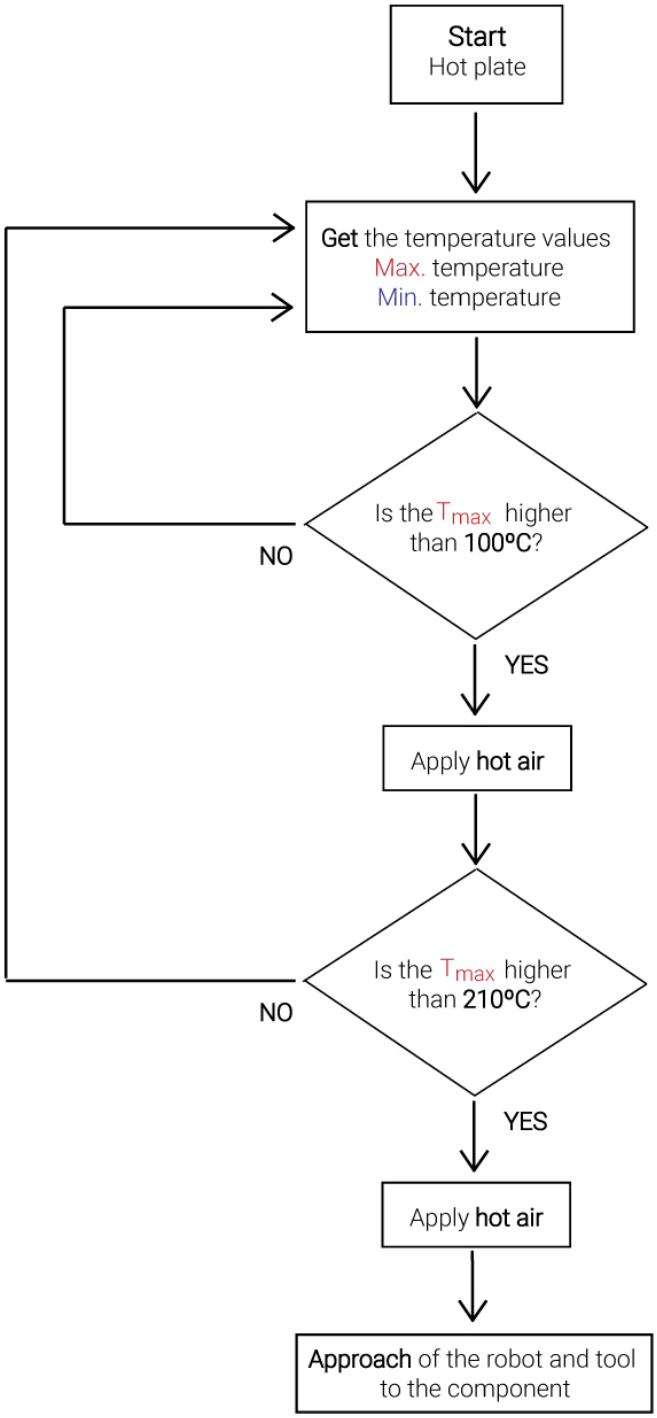

Figure 3.9: Flow chart related to the initial phase with the thermal camera.

In Figure 3.10, there is a diagram associated with the algorithm related to the robotic interaction control phase of the tool with the component and board. The values chosen (force and position) to detect the moment when the weld melts are related to the maximum magnitude of the force and position displacement vectors observed in the tests.

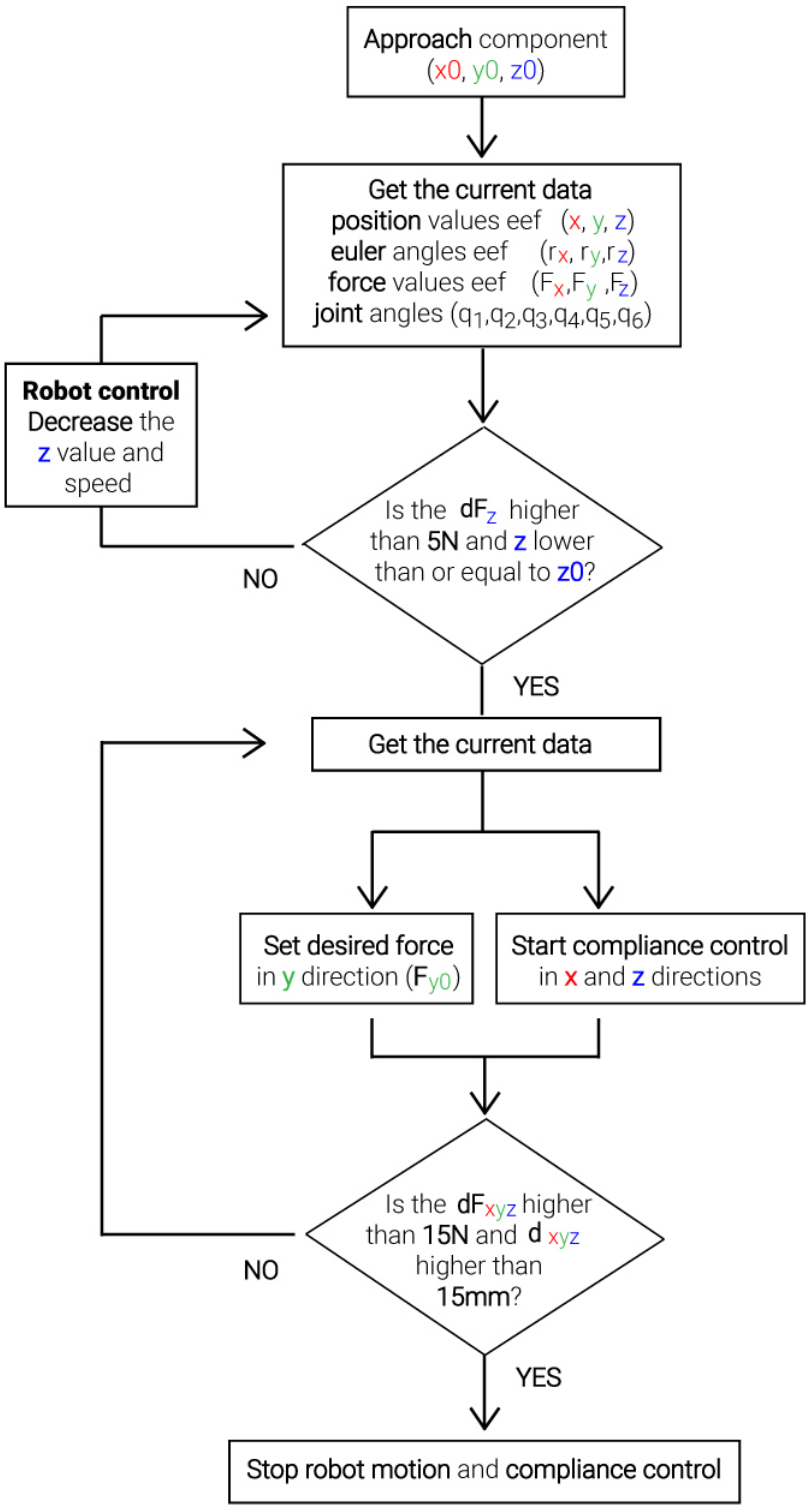

Figure 3.10: Flow chart related to the robotic interaction control of the tool with the component and board phase.

As already mentioned, the initial position of the component's contact point (x_0,y_0,z_0), that takes into account the size of the tool, l_c (Figure 3.11), and the predefined gripper's aperture, a_g (Figure 3.11), was introduced manually using the Teach Pendant. It is important to note that the function's input value, a_g, that controls the gripper opening corresponds to the sum of the distance between the fingers, a_i (Figure 3.11), and associated fingers offset, d_{off} (Figure 3.11). So, later with the vision system's introduction of the component's contact point poses (x_c, y_c,z_c), concerning the referential of the Base, the y coordinate to be input in the system should be calculated by the equation 3.6, y_{new} (Figure 3.11).

$$y_{new} = y_c - (\frac{a_i}{2} + \frac{d_{off}}{2} + l_c) \tag{3.6}$$

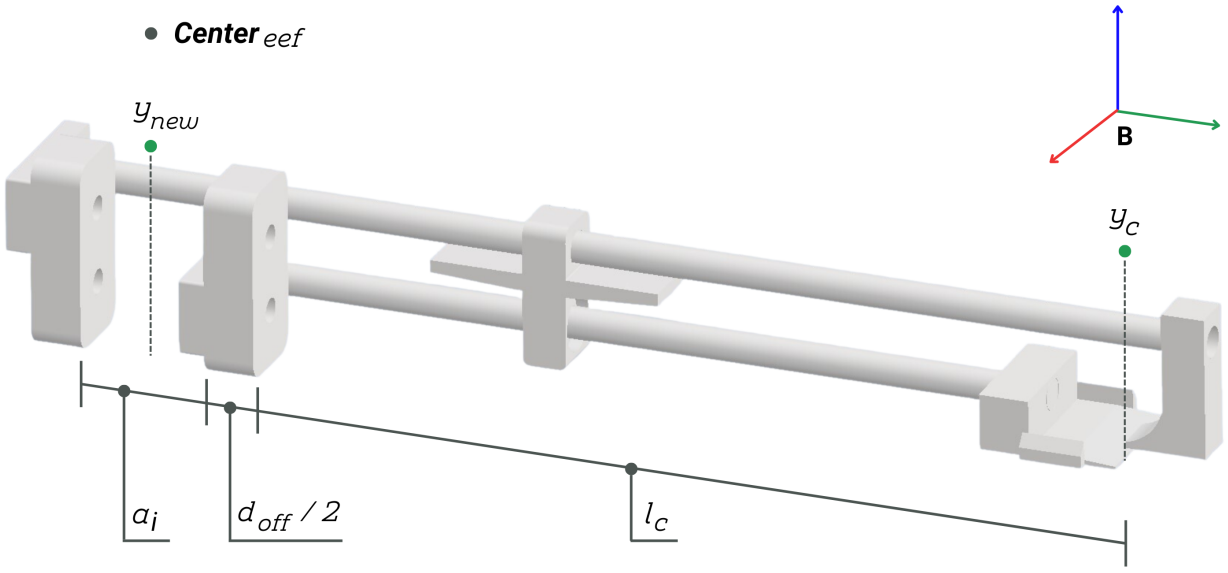

Figure 3.11: Representation of the y-coordinate of the end-effector in the situation where the pose of the component is given directly to the system.

Finally, Figure 3.12 represents the algorithm associated with the component grasping, transport, and release phases, previously described in the path planning section. In the grasping step, the value of the gripper opening, defined as the limit (a_g equals 75 millimeters) to finish this operation, corresponds to the situation where the tool's two final parts 4 and 5 touch each other (Figure 3.5).

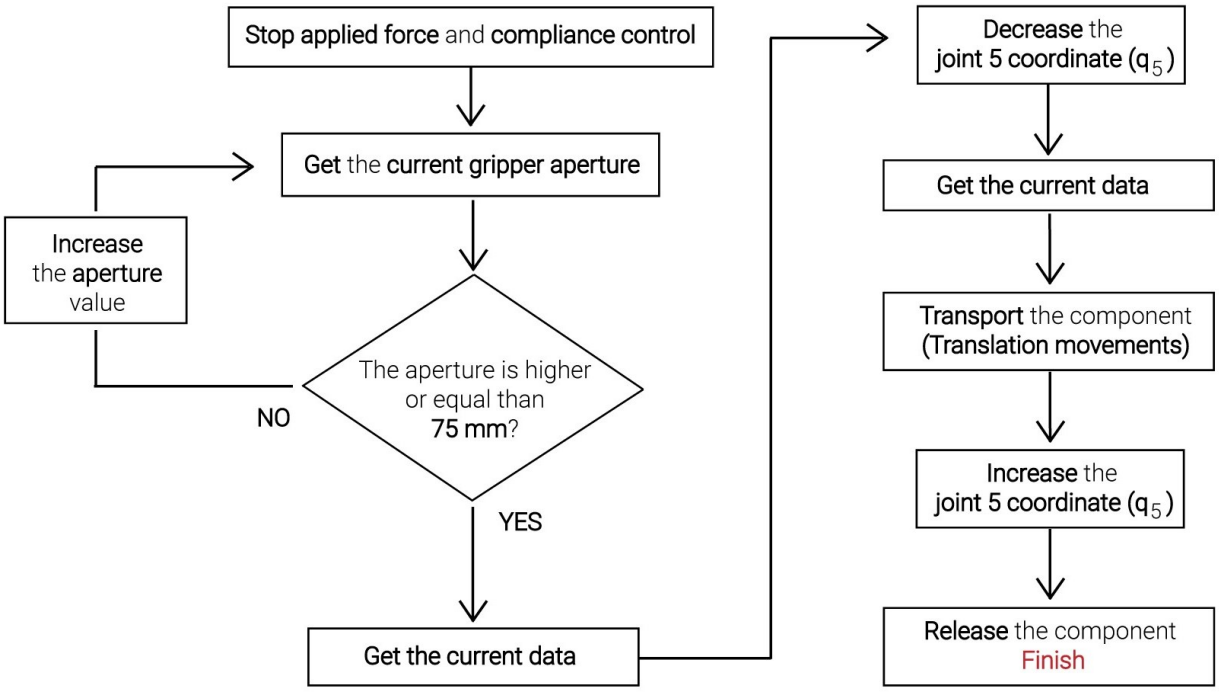

Figure 3.12: Flow chart related to the robotic interaction control of the grasping, transport, and release phases.

3.7.3 ROS architecture

As mentioned, the entire algorithm was implemented in ROS. In this way, two nodes were created:

- Subscriber node ('/dsr_example_py') that subscribes to the topics ('/dsr01m1013/state/') that provide the data associated with the current state of the robot and the topic created exclusively to receive the data from the thermal camera. All topics exchange messages of type float.

- Publisher node ('/thermal_cam') that publishes the temperature data, maximum and minimum values, in the developed topic ('/min_max_temp').

The Figure 3.13 shows the implemented architecture.

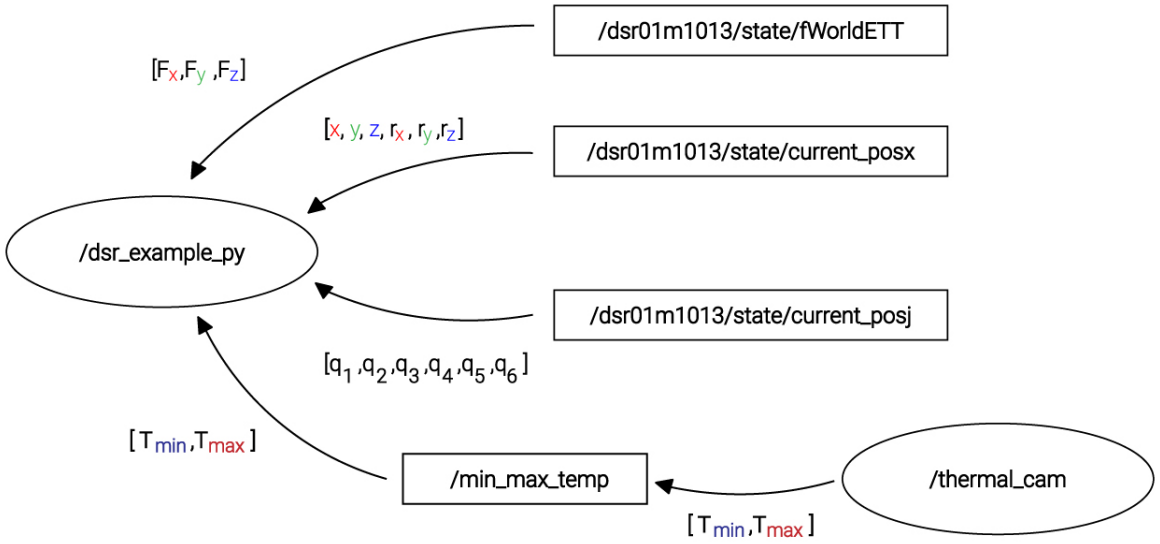

Figure 3.13: ROS map.

Chapter 4

Results and discussion

This chapter presents the main results obtained relative to the different phases of the process and their respective discussion. In turn, it is structured in the following sections.

1. Tool, where the manufactured prototypes (Prototype 1, Prototype 2 and Prototype 3) are presented and described, and their performance is evaluated.
2. Force control, in which the precision and accuracy associated with the force data during the contact with the component are analyzed.
3. Tests with a single contact point tool, that present the results needed to evaluate the behavior of the force data in a first approach to the problem.
4. Level 1: Tests with PCB components attached to a clean surface, where the data that describes the disassembly process in components fixed with hot glue is presented.
5. Level 2: Tests with the larger PCBs, which are the results of the robotic disassembly applied in components of these types of PCBs.
6. Level 3: Tests with cell phone's PCBs, that has the same structure as the previous subsection but at the cell phone PCBs' components domain. It is shown the components extraction process results, which is the main goal of this study.

All values acquired by the sensors integrated into the manipulator and used are relative to the end-effector and the Base coordinate system (Figure 3.1).

Regarding the first section, the results associated with the fabricated tool are presented, including all the versions that it assumed throughout the execution time of the study. Then, each version's practical advantages and disadvantages are mentioned, and their performance is analyzed. Next, the force data relative to the contact phase (before the component starts to move) are presented to discuss the precision and accuracy associated with the force control. Afterward, the force and position values, corresponding to the data collected in a setup with a single contact point tool, that describe the system behavior in the contact and desolder moments are shown and discussed. These previous tests were necessary to develop the algorithm used in the following tests that implemented the whole operation.

Finally, the presented results describe the whole disassembly process (position and force values), applied in three conditions corresponding to three different difficulty levels. This test's structure is because, as the study integrates a system with several phases, it is beneficial to

gradually increase the difficulty of the test conditions to improve the system as it approaches the situation associated with the study's final application. Based on that, the entire operation was performed first on components attached to a clean surface (Level 1) without surrounding components. The choice of hot glue for an initial phase was related to its behavior being identical to that of the solder when melted. It also has a lower melting point, which speeds up the extraction process, reduces the execution time of the tests, and allows high repeatability of the tests since the conditions were easy to replicate from test to test. Levels 2 and 3 of difficulty corresponded to tests performed on larger printed circuit boards, which means more space between components and larger components and cell phone PCBs (final stage). Figure 4.1 shows the base setup used in all the tests performed.

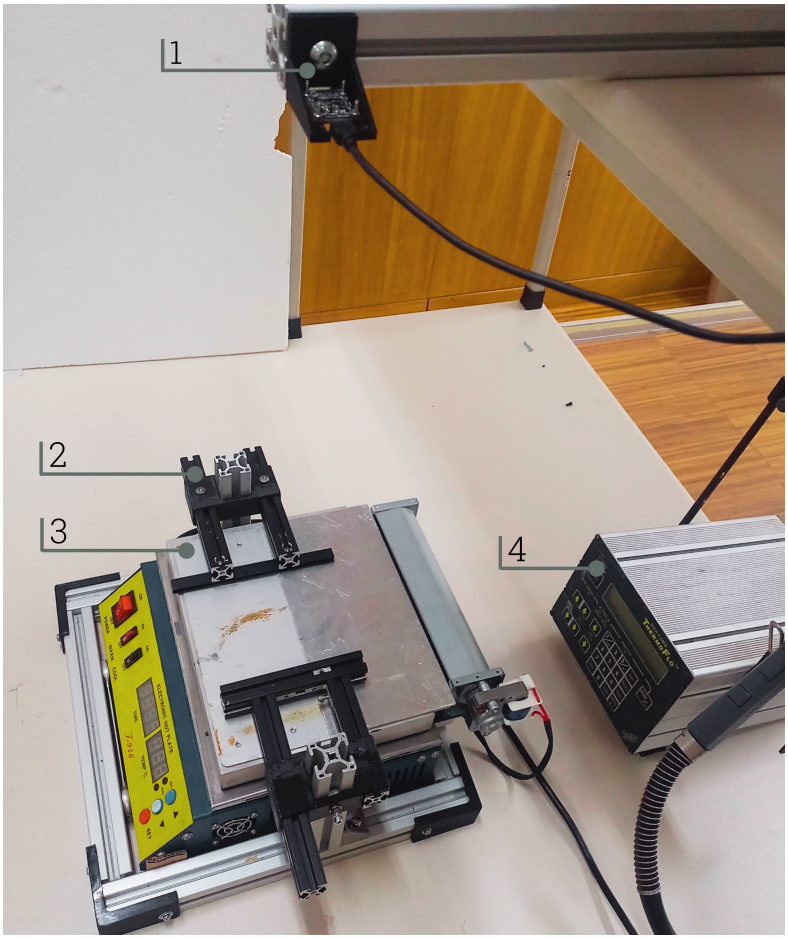

Figure 4.1: Experimental setup for the robotic disassembly operation of printed circuit board components. (1) thermal camera, (2) support for the boards, (3) hot plate, and (4) hot air device.

4.1 Tool

As mentioned, the tool design shown in the Figure 3.5 has taken on different versions. At first, all the tool parts were manufactured using additive manufacturing (Prototype 1 shown in Figure 4.2), except for the galvanized steel bars that support its entire structure (number 3 in Figure 3.5).

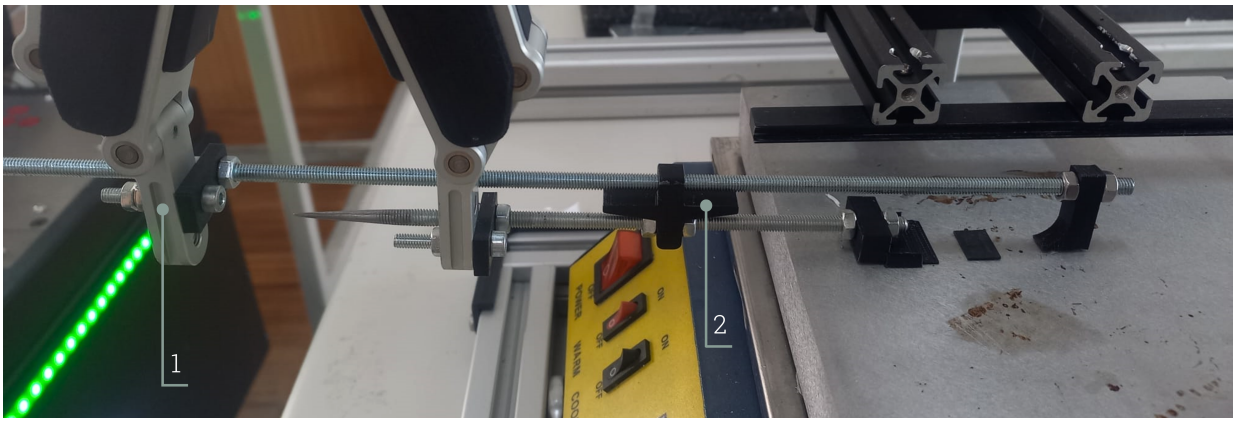

Figure 4.2: Prototype 1 of the tool fabricated to remove PCB's components. (1) gripper, and (2) tool.

The tests made with this prototype were intended to test the architecture and the mechanism's (3.6) performance in the grasping operation, with components already free on a clean surface. This prototype's final parts (parts 4 and 5 in Figure 3.5) have a higher thickness than expected for the final version to give more stiffness to the tool, which would not be achieved with a smaller thickness of the material used (PLA). Also, the angle in part 4 of Figure 3.5 is not present in this version since it was tested on free components with no obstacles around. Besides that, the flat face facilitates the execution and quality of the printed part.

Prototype 2 of the tool is shown in Figure 4.3. This one has parts 1 and 2 of Figure made of galvanized steel (Figure 4.4), which makes it possible to subject to high temperatures and test it in a real-life scenario of removing components from PCBs (tests of Levels 2 and 3). Part 4 of Figure 3.5, unlike Prototype 1, already has the angle that allows components behind the one of interest not to affect the process. However, due to the limitations imposed by the manufacturer (small size and difficulty in handling), the flat part design was not included in this tool prototype. The remaining parts of the tool remained the same as in Prototype 1 since, due to the tool's architecture, they are not subjected to temperatures that lead to their fusion during operation. This detail reduced the costs associated with the fabrication process.

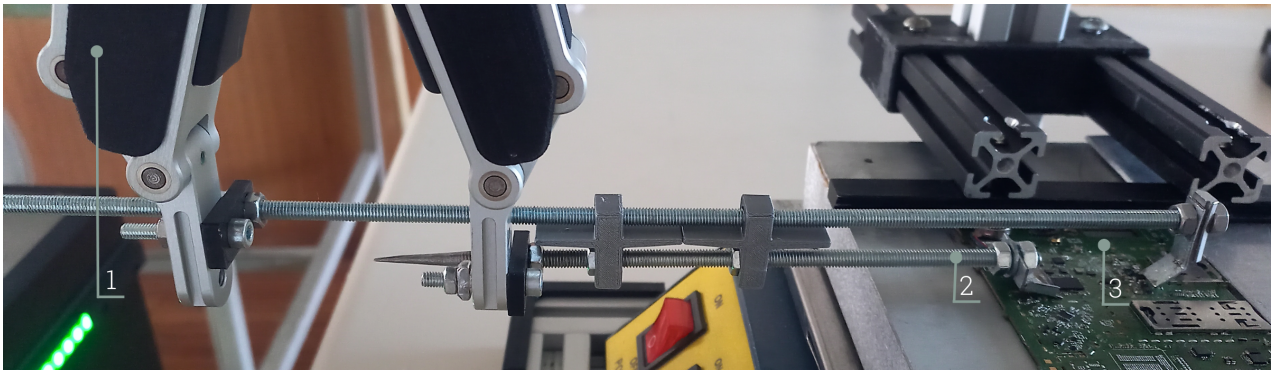

Figure 4.3: Prototype 2 of the tool fabricated to remove PCB's components. (1) gripper, (2) tool, and (3) mobile phone's PCB.

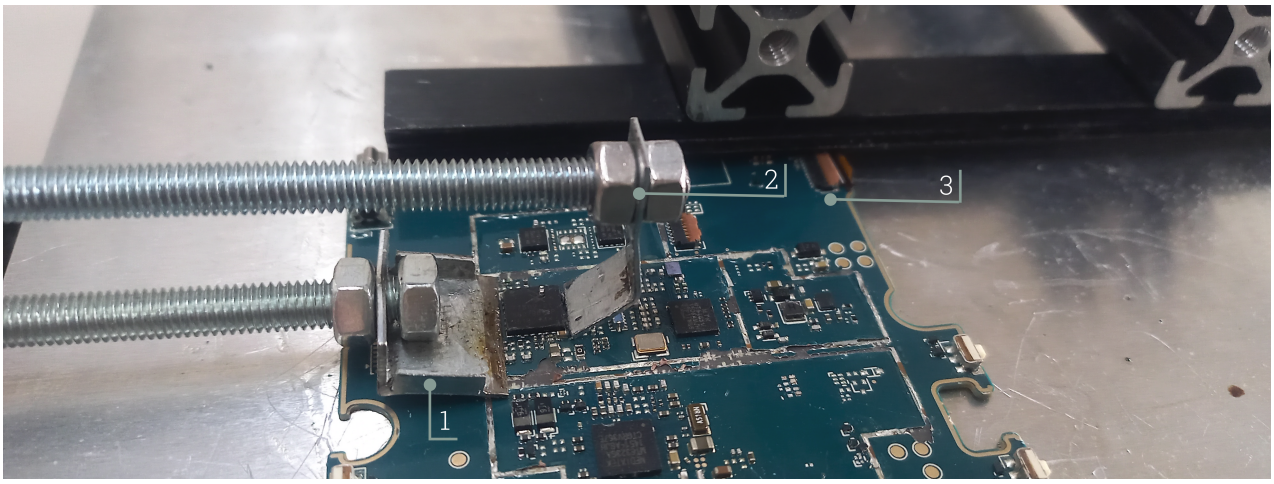

Figure 4.4: Grasping parts of Prototype 2 of the designed tool. (1) receiving part that also applies the extraction force, (2) the end part that ensures that the grasping process is performed, and (3) the mobile phone's PCB.

As Figure 4.3 shows, an additional intermediate part has been added in Prototype 2 to give the tool more stiffness.

Figure 4.5 is Prototype 3 of the tool based on the previous one since only part 4 of Figure 3.5 was modified. This modification in the mentioned part aimed to reduce the contact area of the tool with the component to extract (keeping the type of contact assumed line-plane) to decrease the contact with other components on the sides, verified in tests performed with Prototype 2. In addition, the thickness of the final section of part 4 (Figure 3.5) was reduced, allowing it to fit into even narrower component gaps. The edges that support the component removed during the grasping operation do not appear in Prototype 3 since it was manually fabricated in the laboratory. It was included in the tests, and it was possible to test its performance in the contact phase and start of grasping.

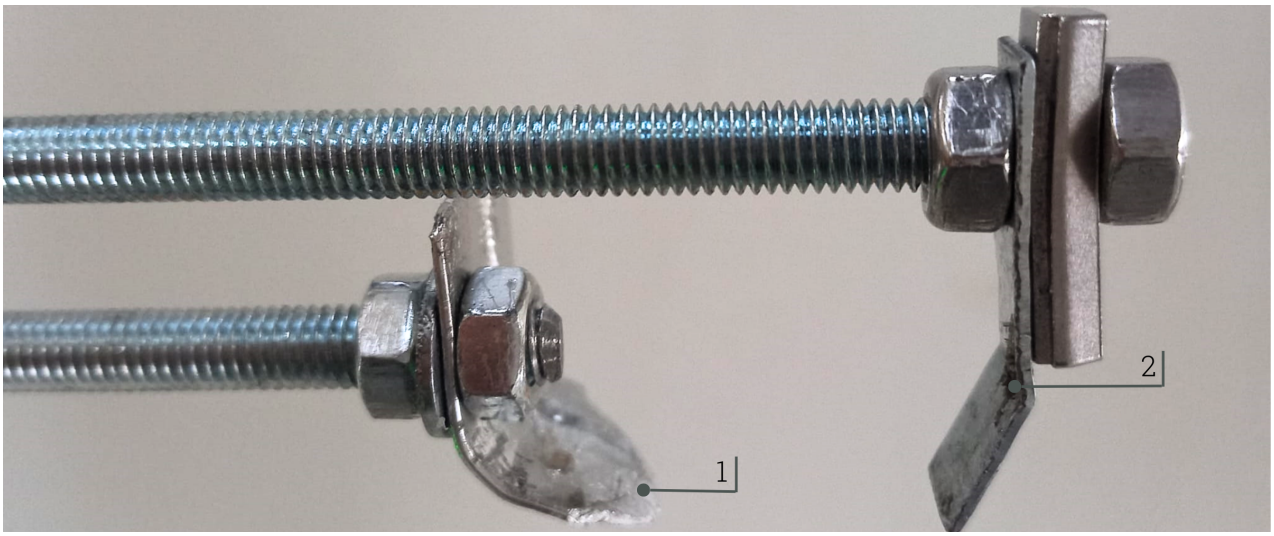

Figure 4.5: Grasping parts of Prototype 2 of the designed tool. (1) receiving part that also applies the extraction force, and (2) the end part that ensures that the grasping process is performed,

Table 4.1 summarizes the performance of each tool prototype based on the tests performed. Prototype 1 4.2 was tested on grasping PCB components previously desoldered and free on the setup. Prototypes 2 and 3 were also tested under the same conditions as the previous prototype and subjected to conditions of the tests with PCB components attached to a clean surface (Level 1), only the grasping phase of the algorithm. Under these last conditions, based on the testing history, in ten tests performed for each, the component grasping operation was completed in six for Prototype 1 and seven for Prototypes 2 and 3. Available cell phone boards were not used in this testing performance phase. The last two prototypes (Prototypes 2 and 3) of the tool were tested on the PCBs when the whole algorithm was already implemented to save essential resources for the final tests.

The parameters indicated in the table directly affect the viability and applicability of the tool in the execution of the proposed operation. Therefore its reading allows a qualitative analysis of the performance underlying it.

Table 4.1: Comparison of the tool prototypes' performance in key robotic component disassembly operation requirements.

Prototype	Tolerates temperatures above 200ºC	Appropriate contact thickness	Appropriate contact area	Appropriate angle	Stability in the grasping operation
1	X	√	X	X	√
2	√	X	X	√	√
3	√	√	√	√	X

Considering the information in Table 4.1, it is possible to conclude that only the prototypes made of galvanized steel (Prototypes 2 and 3) are viable for the application at hand (qualitative analysis). Furthermore, the one that meets the most requirements necessary for the success of the process is Prototype 3 of the fabricated tool (Figure 4.5). However, it would be necessary to introduce sidebands and improve the tool architecture to provide the stability required to complete the operation.

4.2 Force control

This section presents the data concerning the values of the constant force, F_{y0}, exerted in the direction defined for extracting the component in the phase immediately before the desoldering. It is essential to mention that the module of this force varied according to the conditions in which the test was performed and taking into account if it was necessary to exert more or less force. Thus, a module value of 10 N was set for the tests performed with PCB components attached to a clean surface (Level 1) and 20 N for those performed with the PCBs. Since the behavior of the data is identical in the tests associated with each value of the force set, only one representative case is represented here. The choice of this case was based on the duration of the period during which the force was applied. Thus, the tests chosen were the ones that this period has a longer duration, i.e., in which there is more data for the following analysis, making it more reliable. The data analyzed correspond to the tests performed in the setup not fully warmed under the tests' conditions of Levels 1 and 2. Since the tests performed with the setup already warmed up have this period shorter.

Figures 4.6 and 4.7 show the force values, F_y, in the tool's contact phase with the PCB component, as a function of time associated with the Level 1 and 2 of the tests, respectively. The force values have a negative sign because the measured force corresponds to the one exerted

by the component on the tool and detected by the manipulator (Figure 3.3, $\vec{F_{yc,t}}$), i.e., in the negative direction of the force application direction. For each case, the average of the force values (estimated value of the applied force), $\overline{F_y}$, the respective standard deviation (Equation 4.1), σ, and the associated standard uncertainty (Equation 4.2), $\mu_{\overline{F_y}}$, are calculated to analyze the precision associated with the value of the applied force exerted.

$$\sigma(F_{yi}) = \sqrt{\frac{\sum_{i=1}^{n}(F_{yi} - \overline{F_{yi}})^2}{n-1}} \tag{4.1}$$

$$\mu(F_{yi}) = \sigma(\overline{F_{yi}}) = \frac{\sigma(F_{yi})}{\sqrt{n}} \tag{4.2}$$

where n is the number of force data corresponding to the period of force application. This value varies from test to test since the data associated with this phase is higher or lower depending on the board and the component size. Thus, it will always be different in all tests performed. However, as the number of samples is still high even in tests with this shorter phase (n higher than 1000), an analysis of this type is still valid and essential to understanding the precision and accuracy of the implemented system.

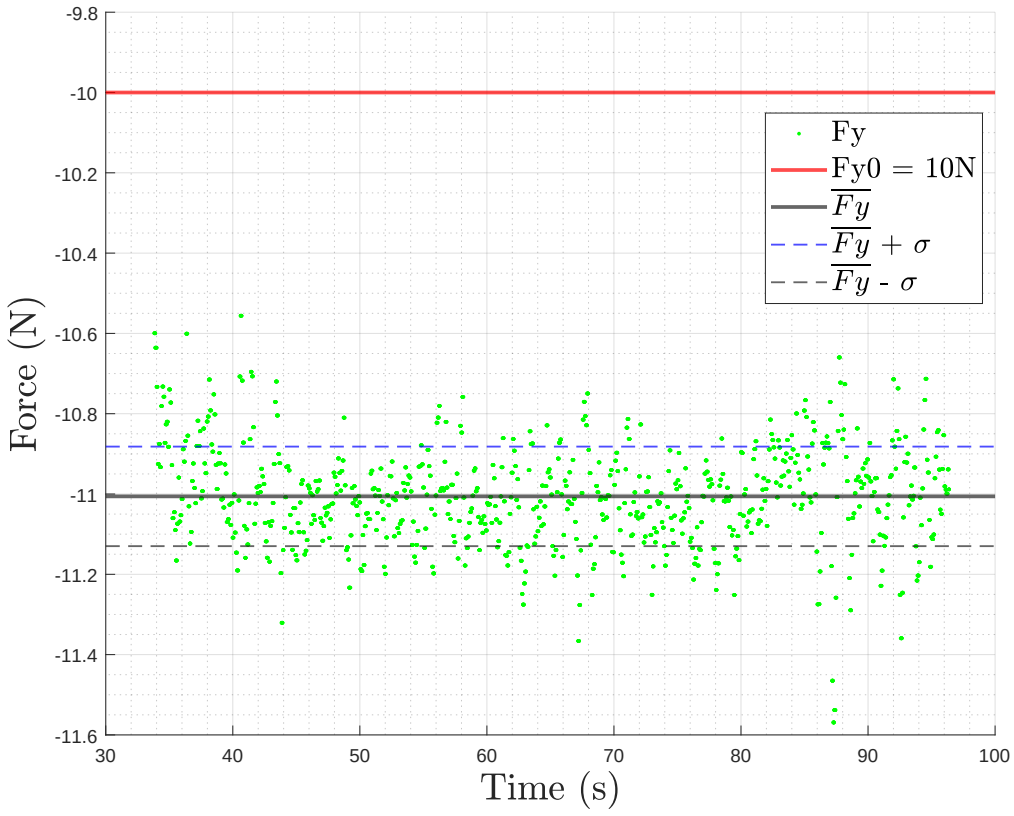

Figure 4.6: Representation of the force values at the contact's phase with the component as a function of time under the conditions of the tests where the operation is performed on PCB components attached to a clean surface (Level 1). The acquisition data rate was 100 Hz.

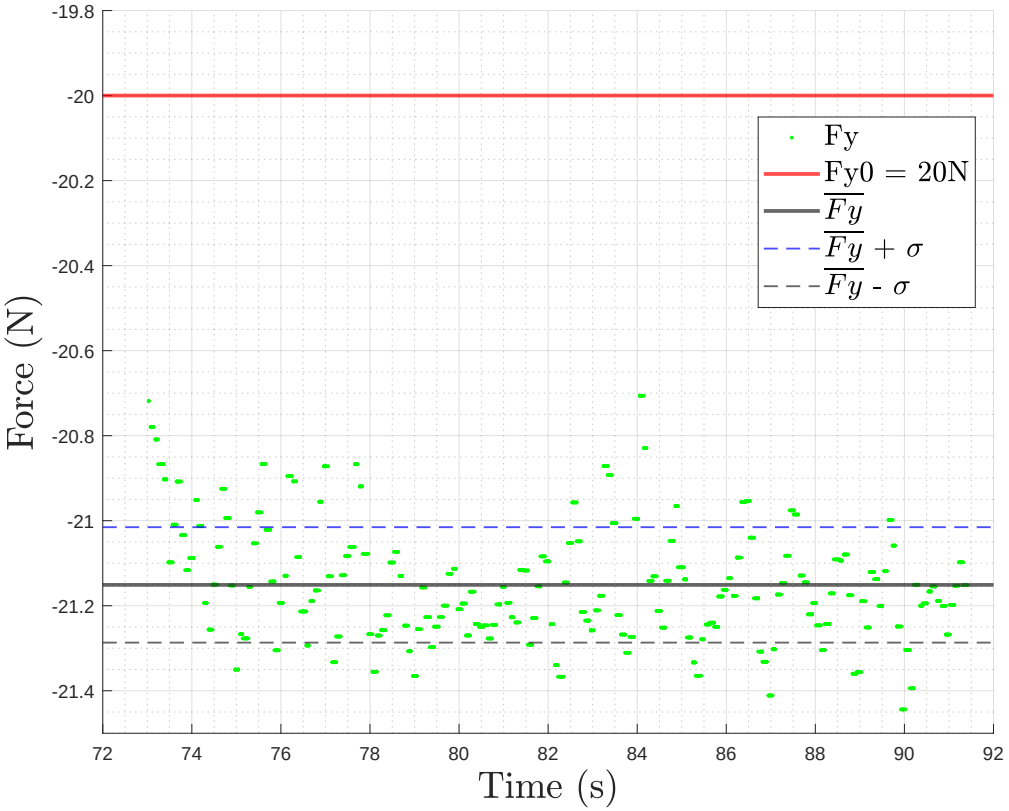

Figure 4.7: Representation of the force values at the contact's phase with the component as a function of time under the conditions of the tests where the operation is performed on components of PCBs (Level 2). The acquisition data rate was 100 Hz.

Table 4.2 presents the values obtained, including the percentage error of the estimated value of the applied force relative to the actual value, *err* (4.3).

$$err(\%) = \frac{|\overline{F_y} - F_{y0}|}{F_{y0}} \cdot 100 \tag{4.3}$$

Table 4.2: Results of the estimated value (mean of the values), standard deviation, and standard uncertainty of the applied force on the component to be removed.

Test' condition	$\overline{F_y}$ **(N)**	σ **(N)**	$\mu_{\overline{F_y}}$ **(N)**	*err* (%)
Hot glue	-11.006	0.124	0.002	11.510
PCBs	-21.015	0.136	0.003	10.059

Regarding the values obtained, it is possible to conclude that the control used has good precision for the application in question since 95% of the measured values tend to disperse in the estimated value in a value range of only 0.2N (2σ). This dispersion associated with the data in the phase in question may be related to random errors associated with the test conditions (collision with other components, for example) and noise sources affecting the circuit implemented in the manipulator's controller. Concerning accuracy, the estimated values vary about 1N from the expected value, which may indicate poor accuracy depending on the application (for applications with more delicate materials, this may be a problem). As this tendency was verified in the various tests performed, this variation is likely associated with systematic errors

inherent in the system, such as miss calibrations. However, for the operation in question, as it removes components with high rigidity, applying much force does not affect the viability of the process.

4.3 Tests with a single contact point tool

For the definition of the threshold values of the conditions that command the flow of the implemented algorithm, it was necessary to perform tests that would allow us to have an idea of the variation of the values of force and position in the situation in which the component desolders, and if this variation was perceptible only with the use of the manipulator's integrated sensors. If this were not the case, it would be necessary to introduce a load cell or other force sensor capable of detecting a variation in values needed to implement the process. Since a load cell was available, it was introduced in the setup (Figure 4.8) intended for this test.

Thus, a sharp rigid bar attached to the gripper was used to exert a force established at a contact point and a PCB with larger dimensions than the cell phones (Level 2). As the test's purpose was only to observe the behavior of the data in the solder melt situation, a tool with a single point of contact was enough.

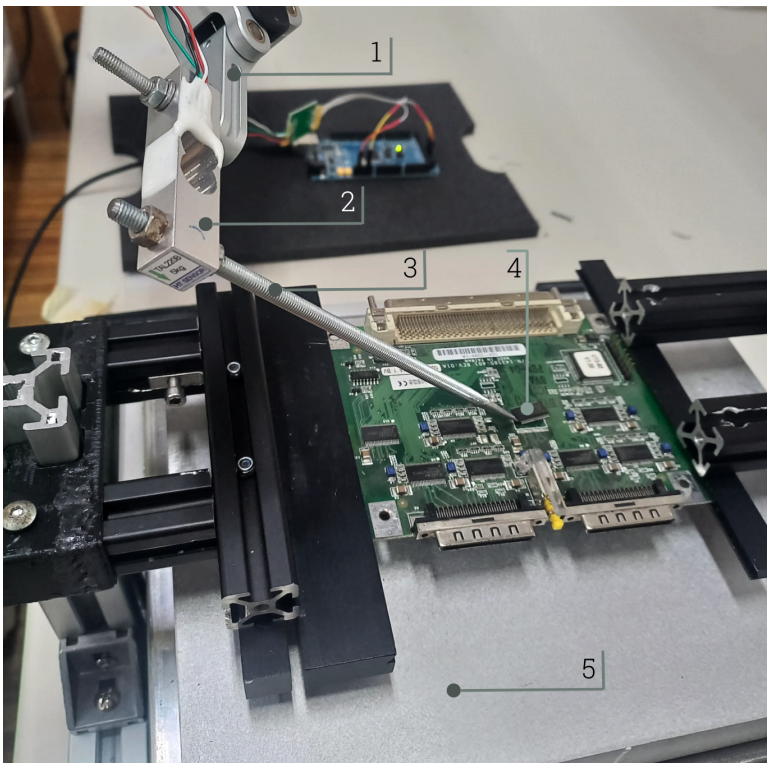

Figure 4.8: Experimental setup for the tests without tool. (1) gripper, (2) load cell, (3) threaded bar, (4) PCB' component, and (5) hot plate.

Although this is a test of a PCB, the force applied to extract the component was only 10N. This force value is because the extracted components, unlike PCBs like those on cell phones, have visible connections, which makes desoldering easier and therefore requires less force. In addition, applying a lower force value allows the displacement of the component to take place more slowly and, consequently, the desoldering phase to be observed in the data in more detail (purpose of the test). Figures 4.9 and 4.10 show the force and position data of the end-effector, respectively, relative to the referential of the robot's Base.

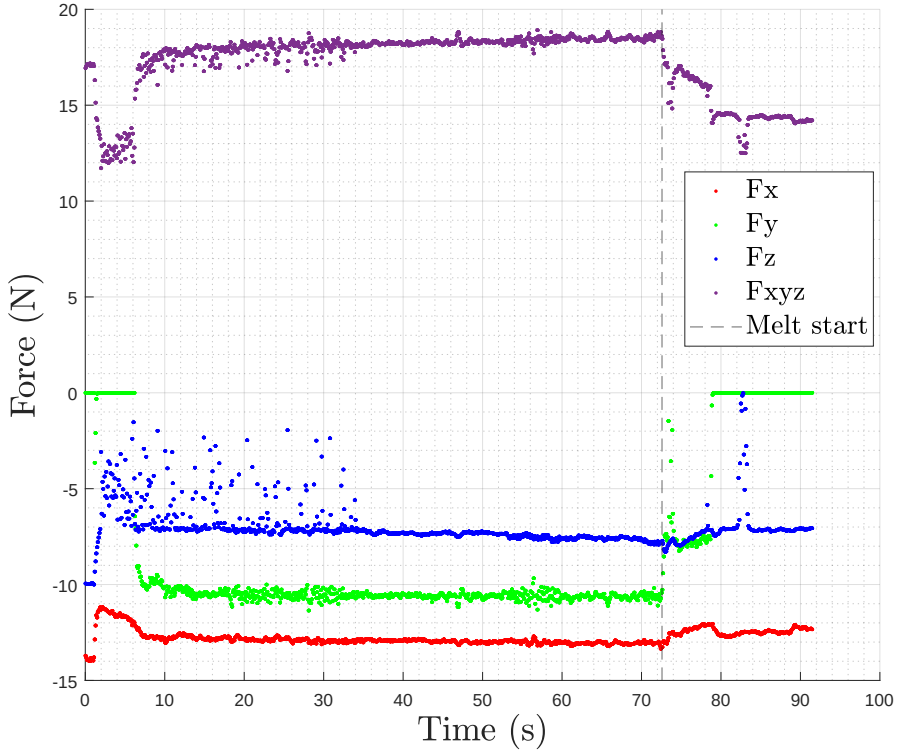

Figure 4.9: Representation of the force values in the component contact and desoldering phases.

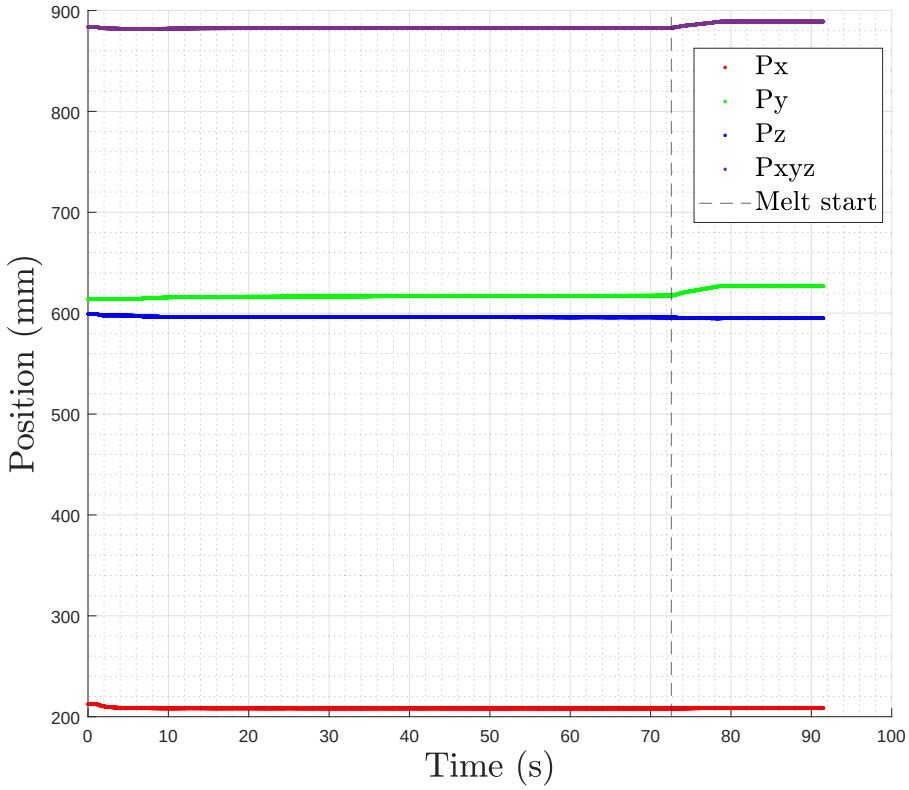

Figure 4.10: Representation of the position values in the component contact and desoldering phases.

Through the previous graphs, it is possible to verify that the desoldering situation is characterized by a decrease (in modulus) of the applied force and an increase in the modulus of the

position vector, which indicates the occurrence of a movement of the component. The values of the modulus of the position displacement vector, d_{xyz}, and the force, dF_{xyz}, used in the implemented algorithm were based on the values observed in this test, these being the minimum values that can be acquired (about 5N for the modulus of the force-displacement vector and 10 mm for the position one). This value varies from case to case, depending on the amount of solder holding the component. However, attending to the present results, it was possible to analyze the behavior of the data and get an idea of values. Furthermore, it is concluded that it is possible to detect the variation of the values by only using the robot's integrated sensors, thus removing the load cell and making the solution more economical.

4.4 Level 1: Tests with PCB components attached to a clean surface

The implementation and testing of the algorithm that includes all phases of the robotic component disassembly operation were first performed on the setups shown in Figure 4.11. In these tests, the desoldering phase was performed using only the hot air device since hot glue melts easier than solder. In addition, if the heated table was used, the component would not fix in the setup, and the force application part with the component static would not be seen. Another aspect is related to the temperature, which indicates the approach of the manipulator in the algorithm. As mentioned, hot glue does not need that much temperature, so the robot is approached when the system exceeds 45 ºC.

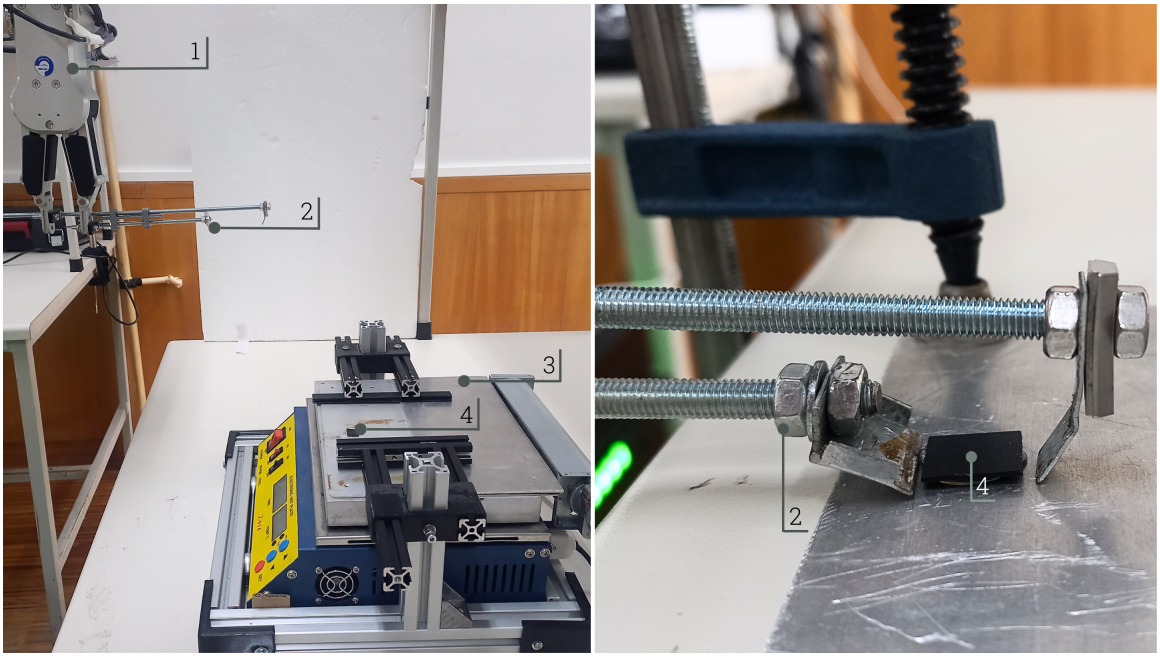

Figure 4.11: Experimental setups for the tests with PCB components attached to a clean surface (Level 1). (1) gripper, (2) tool, (3) hot plate, and (4) PCB' component fixed.

The following is the data describing all phases of the extraction process of the PCB component for two different tests (Test 1 and Test 2) under the conditions mentioned. Figures 4.12 and 4.13, and Figures 4.14 and 4.15 represent the force and position data associated with Test 1 and Test 2, respectively. Although many tests were performed, most of them only completed some phases of the process due to errors inherent to the integration of the whole system (e.g., gripper triggered) and because of the difficulty of grasping objects with a small height as the

components used. Thus, here are only the results of the two tests where the whole disassembly operation was completed.

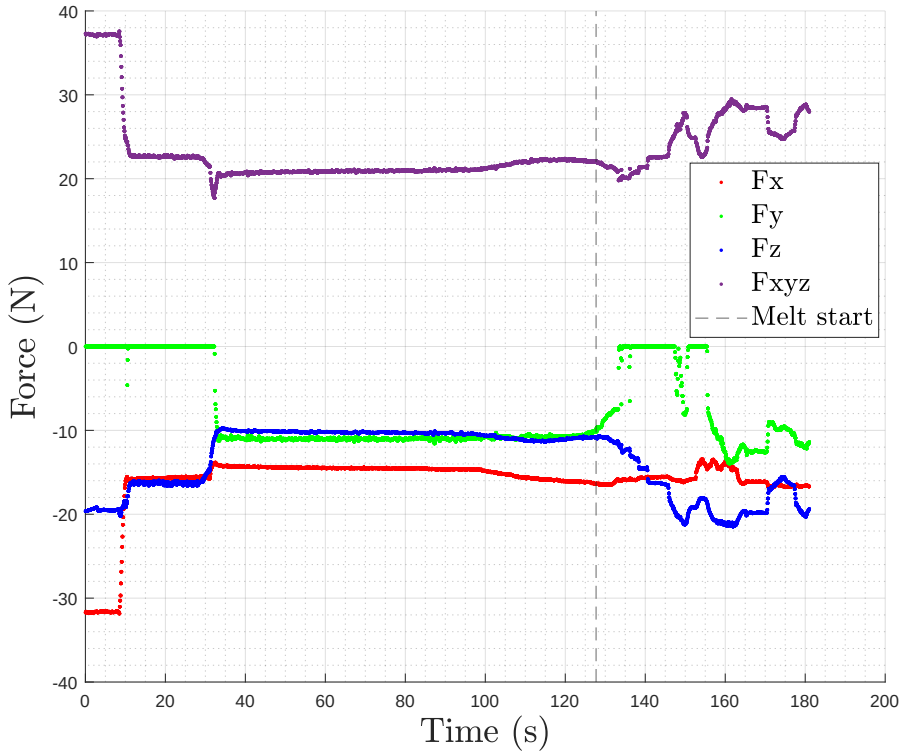

Figure 4.12: Representation of the force values associated with all process phases for extracting a PCB component fixed to a clean surface (Level 1, Test 1).

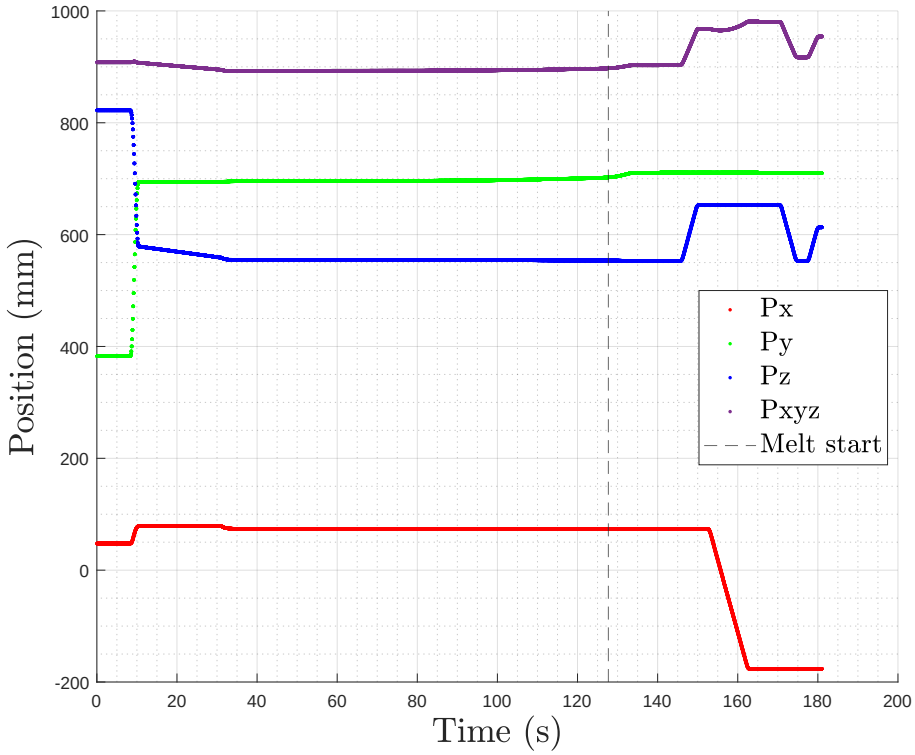

Figure 4.13: Representation of the position values associated with all process phases for extracting a PCB component fixed to a clean surface (Level 1, Test 1).

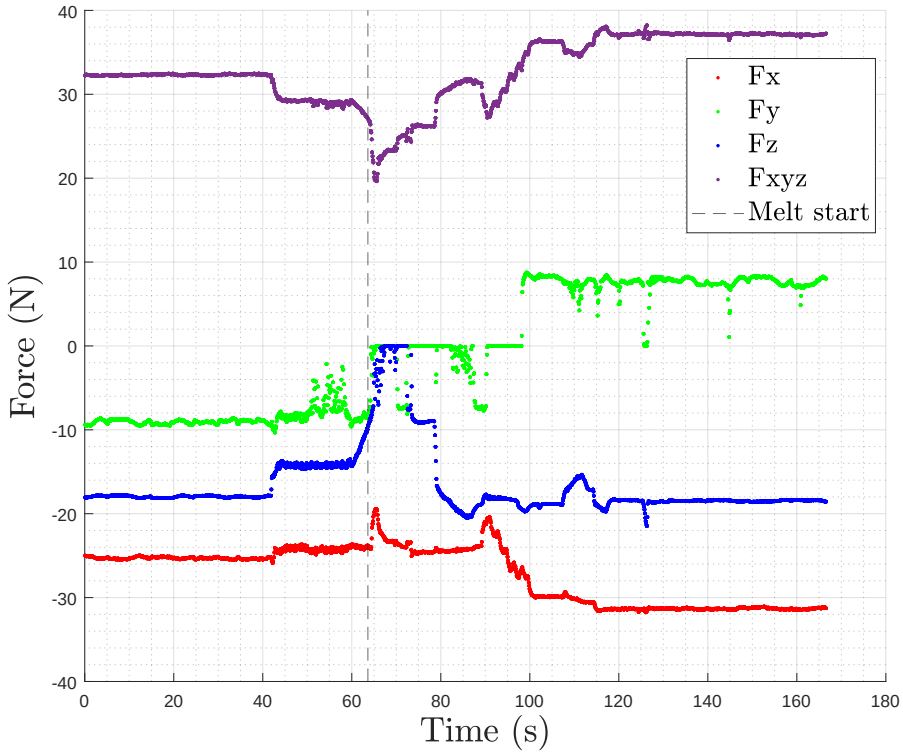

Figure 4.14: Representation of the force values associated with all process phases for extracting a PCB component fixed to a clean surface (Level 1, Test 2).

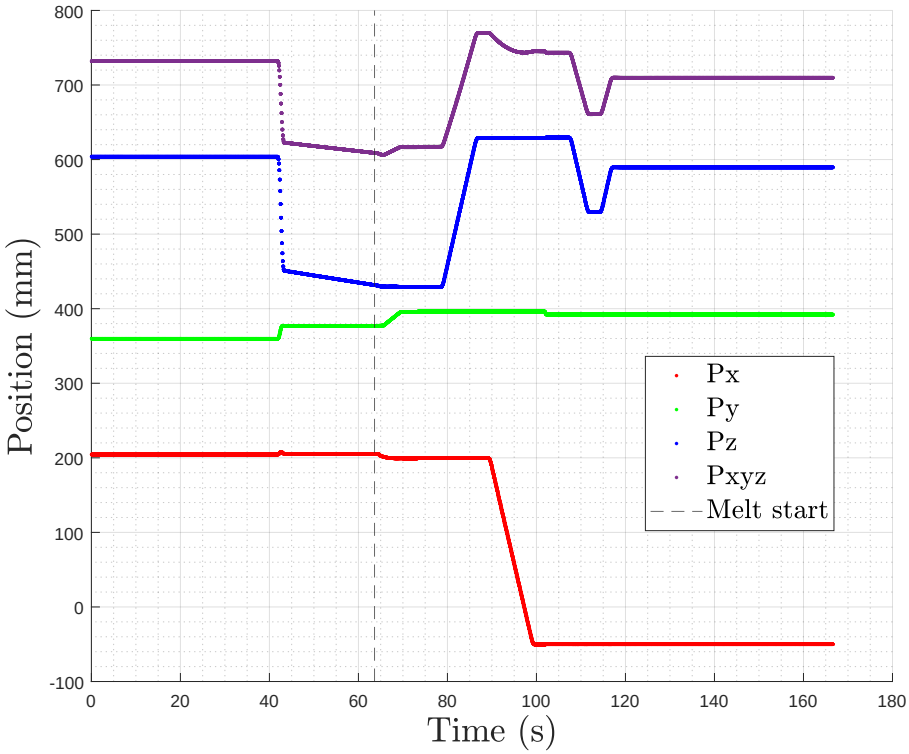

Figure 4.15: Representation of the position values associated with all process phases for extracting a PCB component fixed to a clean surface (Level 1, Test 2).

Table 4.3 identifies the different phases of the process and its approximate duration for both tests.

Table 4.3: Process's phases approximate duration, in seconds, for both tests performed in Level 1.

Process's phase	Test 1 phase's Approximate duration (s)	Test 2 phase's duration Approximate duration (s)
Approach	2	2
Contact	117	21
Melting	6	5
Grasping	12	9
Transport	29	33
Release	3	3
Final movement	3	3

Through the results obtained, it is possible to verify that in both tests, a decrease in the force modulus was observed when the hot glue that fixed the component melted and, simultaneously, an increase in the modulus of the position vector, according to the expected. The period related to the phase in which a constant force is exerted on the component was longer in the first test than in the second, which may be associated with the amount of glue applied to be relatively higher in the first case or associated with the fact that the second test was performed after the first, which meant that the setup had already warmed up slightly, which may have accelerated the melting process. Regarding the sign associated with the force value in the z-axis, this is negative because, in the absence of tool contact, in the end-effector, there is always the gripper and the tool that exert a force in the negative direction of the manipulator's base referential.

4.5 Level 2: Tests with the larger PCBs

Figure 4.16 depicts the setup used for the tests with the larger PCBs (Level 2). In the tests with this type of PCBs, the performance of the transition from desoldering to grasping the components is made very difficult by the surrounding components that deflect the component out of the intended path and by the fact that their height is minimal, making it challenging to start grasping. This aspect was the cause of three of the six tests performed in Level 2's conditions failing in the grasping part. Two tests failed due to system integration errors, i.e., gripper drive failure and unexpected manipulator stop. So, although the procedure was tested on several boards identical to the one in Figure 4.16, only the test shown completed all the steps and is, therefore, the only one whose results are presented here. However, it is important to mention that all the tests performed and the tests at Level 1 complete the desoldering phase.

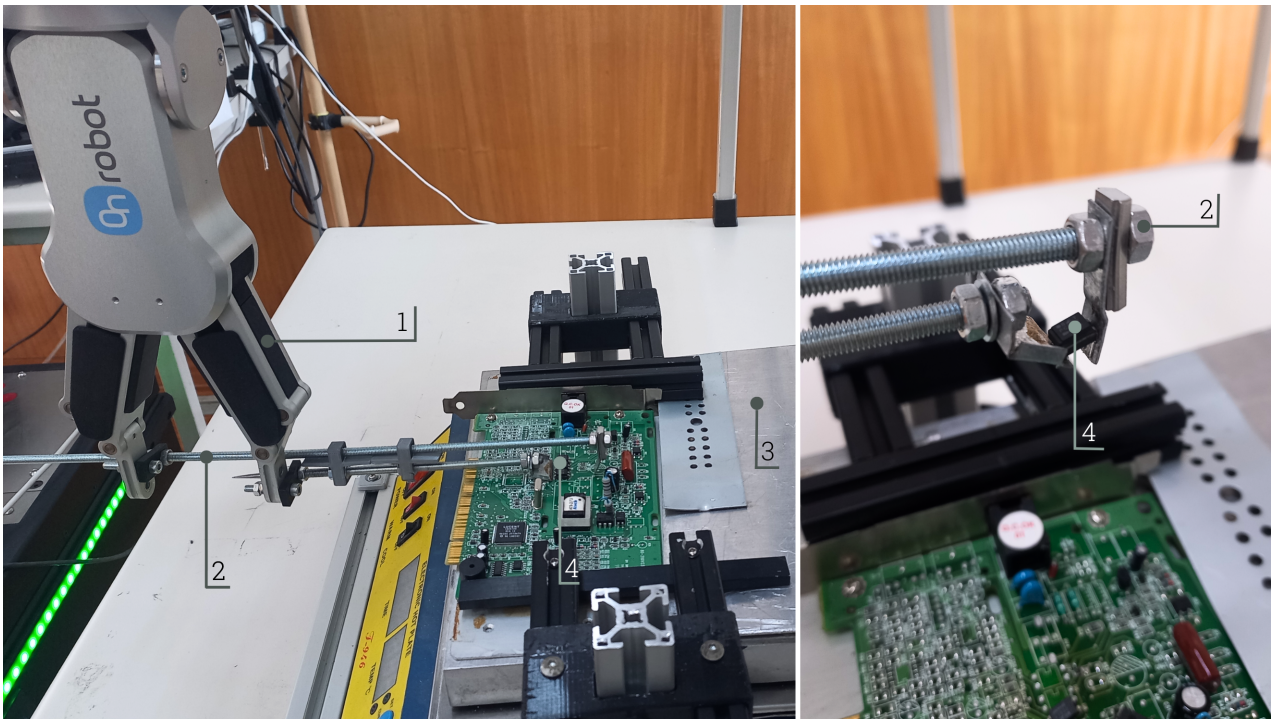

Figure 4.16: Experimental setup for the tests with larger PCBs (Level 2). (1) gripper, (2) tool, (3) hot plate, and (4) PCB' component.

Below are the force (Figure 4.17) and position (Figure 4.18) data describing all phases of the component extraction process relative to the test performed.

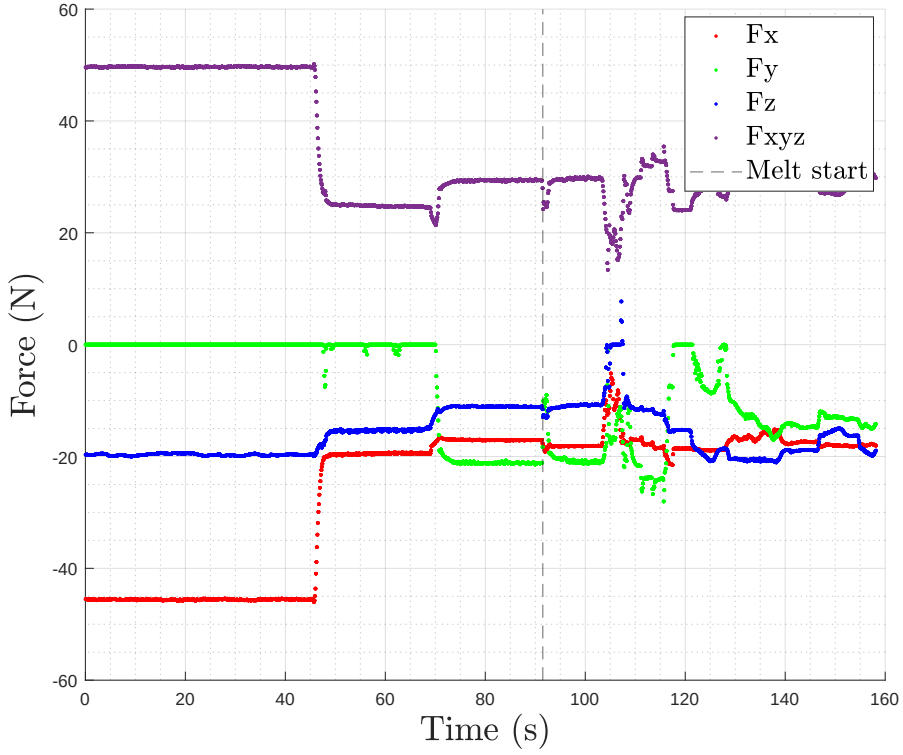

Figure 4.17: Representation of the force values associated with all process phases for extracting a larger PCB's component (Level 2).

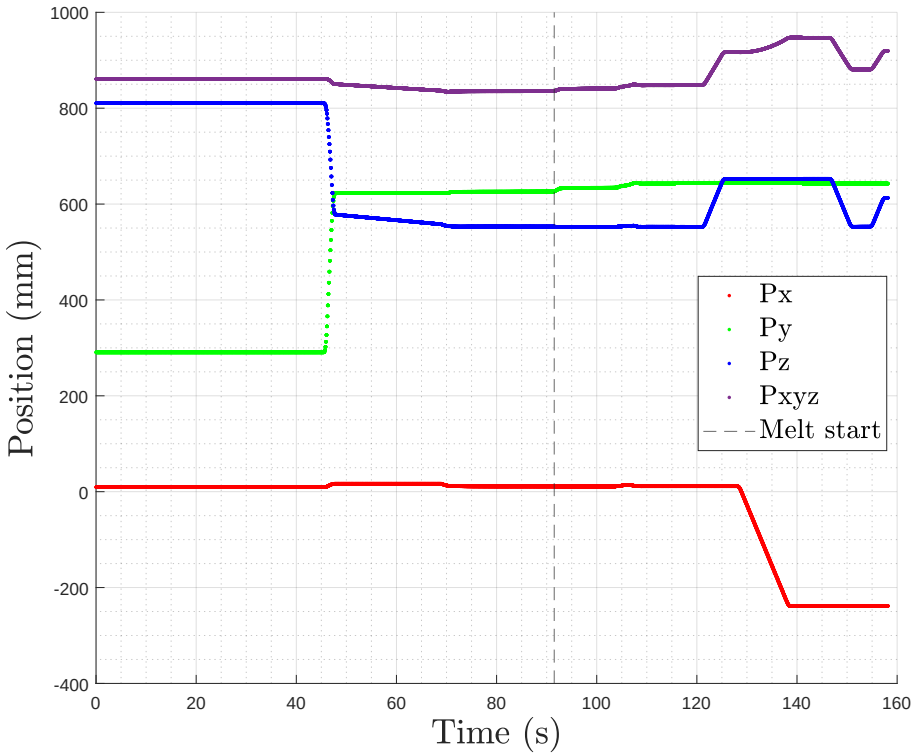

Figure 4.18: Representation of the position values associated with all process phases for extracting a larger PCB's component (Level 2).

As with the tests performed under Level 1's conditions, an approximate duration, in seconds, of each process phase that occurred is recorded in Table 4.4 for a more straightforward analysis.

Table 4.4: Process's phases approximate duration, in seconds, for the tests with larger PCB's components (Level 2).

Process's phase	Approximate duration (s)
Approach	2
Contact	44
Melting	16
Grasping	14
Transport	29
Release	4
Final movement	4

Analyzing the results obtained, it is possible to observe that the trend observed in the force and position data in the previous tests is maintained. However, the phase associated with melting the solder took longer under these test conditions. When the force module decreases, the system quickly continues applying force in the extraction direction, and the component is only desoldered after ten seconds. This delay may be related to the amount of solder that connected the component to the board or to the presence of components in the component's seams preventing it from moving forward. The start of the compliance control and application of the extraction force at instant $\approx$ 72 seconds coincides with the end of the variation of the modulus of the z component of the force ($\vec{F_{zb,t}}$ in Figure 3.3) that indicates that contact has been made between the tool and the board.

4.6 Level 3: Tests with cell phone's PCBs

In this subsection are the results of implementing disassembly operation in cell phone PCB's components. Only Prototype 3 of the tool (Figure 4.5) was used in these tests since it had the best characteristics (e.g., contact area, tool thickness) for extracting the components. As with the tests with the larger PCBs, these tests also had the same challenges but on an even smaller scale. So of the four tests performed on the available cell phone boards, only one successfully completed the entire disassembly process, from contact to release phases. In the others, there were challenges in the transition from desoldering to grasping. In one case, the component's height was so small that the manipulator ran over the component. Based on that, only the results associated with the successfully extracted component are presented in this section. However, as for the tests in Levels 1 and 2, it is important to refer that all the components under Level 3's conditions completed also the desoldering phase. Figure 4.19 shows the setup used for the tests.

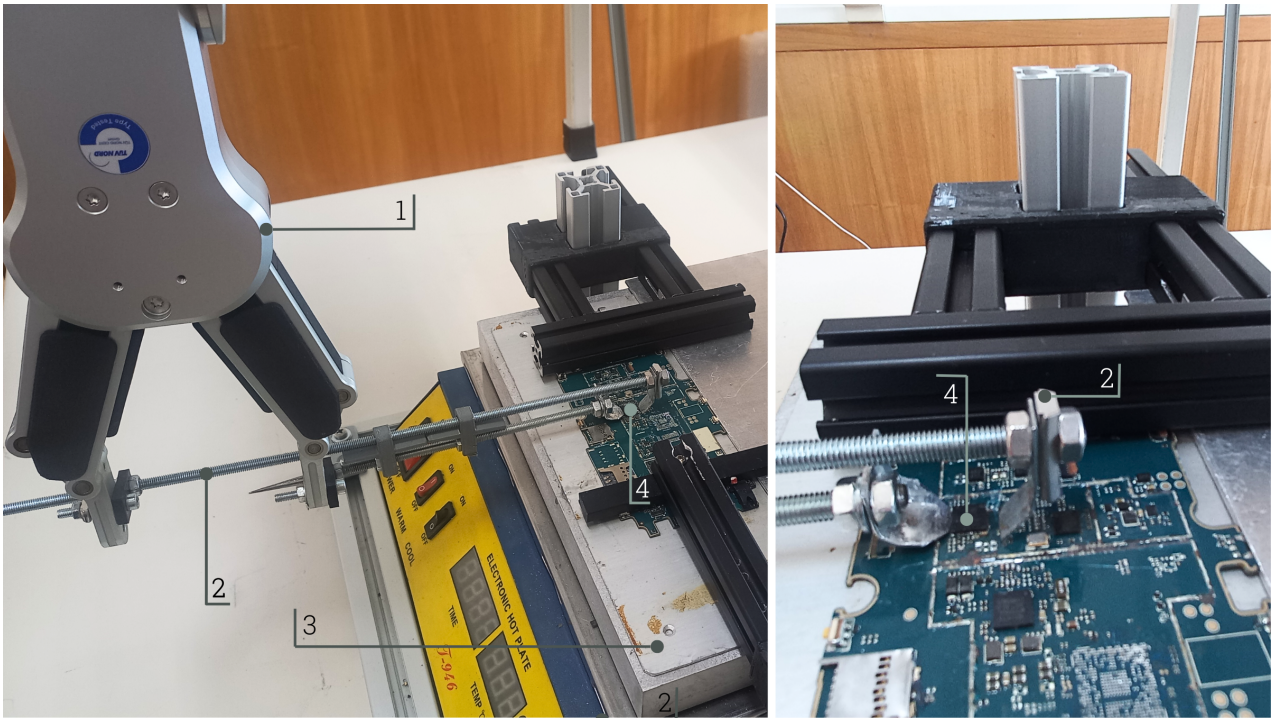

Figure 4.19: Experimental setup for the tests with cell phone's PCBs (Level 3). (1) gripper, (2) tool, (3) hot plate, and (4) PCB' component.

Figure 4.20 and Figure 4.21 are the force and position data associated with all phases of the component extraction process relative to the test successfully performed.

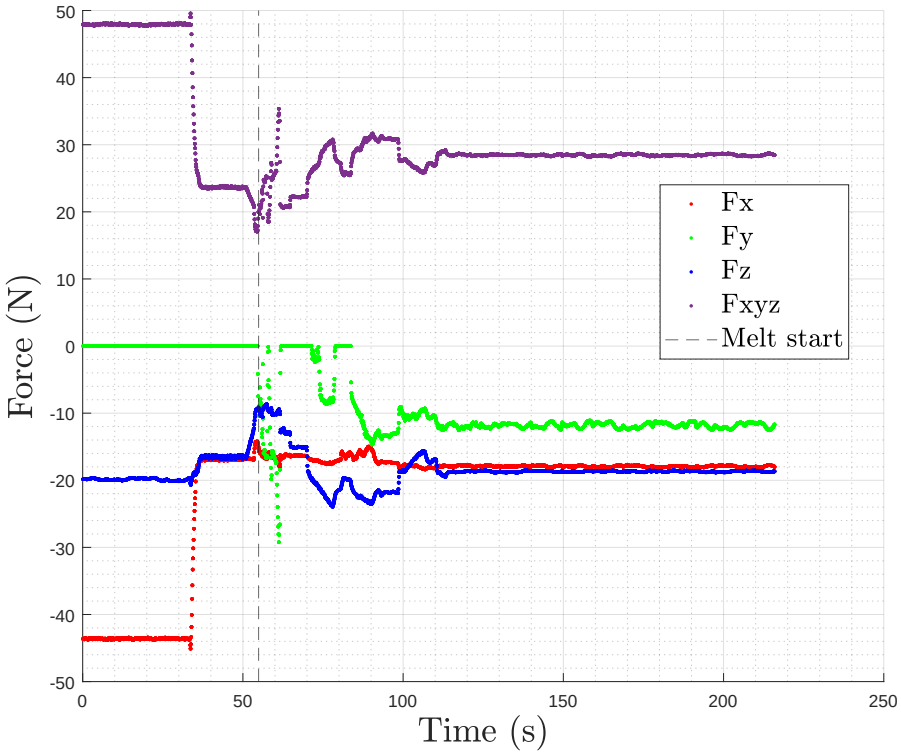

Figure 4.20: Representation of the force values associated with all process phases for extracting a cell phone PCB's component (Level 3).

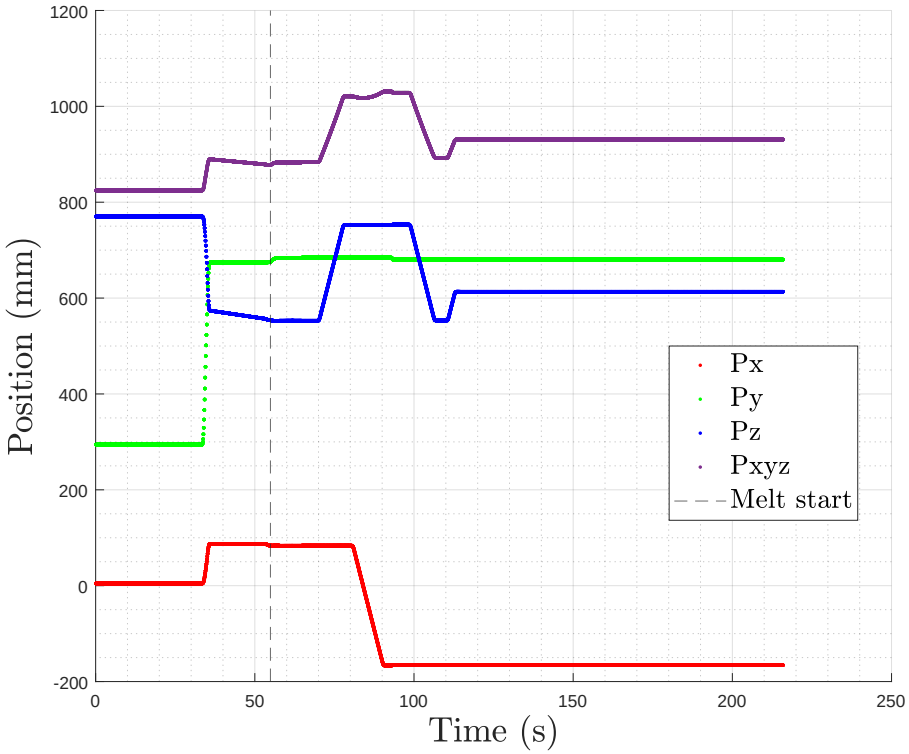

Figure 4.21: Representation of the position values associated with all process phases for extracting a cell phone PCB's component (Level 3).

Table 4.5 identifies the different phases of the disassembly process and their respective approximate duration for the presented test.

Table 4.5: Process's phases approximate duration for the tests with cell phone PCB's components (Level 3).

Process's phase	**Approximate duration (s)**
Approach	2
Contact	7
Melting	4
Grasping	13
Transport	37
Release	4
Final movement	3

The results show that the force application phase after the tool has made contact with the component is almost imperceptible. It is because this test was performed after a few attempts and, therefore, after a lot of hot air application and hot plate action, which results in a component practically unsoldered. Thus, an increase in force modulus is observed in the attempt to reach 20 N, but the component desolders, and the gripping phase are quickly initiated.

Chapter 5

Conclusion and Future work

The main goal of this study was to implement a robotic system that would automate the disassembly of components from cell phone PCBs. To achieve this, the necessary hardware was developed and integrated. This involved using a Doosan collaborative robot with torque sensors in all joints, a thermal camera for real-time monitoring of the system's thermal state, a hot plate, a hot air device, and an Onrobot gripper. The software implementation utilized ROS for the entire algorithm, while Inventor was used for the CAD design of the projected tool's parts.

In order to extract the components, a tool was designed to safely and automatically remove and grasp the PCB components. The tool was also intended to compensate for the imprecisions associated with the gripper. The mechanical principle for the tool's operation was based on leveraging existing resources available in the laboratory, including the gripper and the metals to fabricate it. However, since the desoldering process is detected through variations in force and position values applied to the tool during the hot air application, the tool needed to be in constant contact with the component and therefore exposed to high temperatures.

The tool's performance was initially tested on free components and PCB components attached to a clean surface, which demonstrated a success rate associated with the grasping task of approximately 70%, for the prototypes made of galvanized steel (Prototypes 2 and 3), under those conditions. Subsequent tests focused on examining the force behavior and position data during component desoldering, verifying that the expected variation trends were observed. Threshold values for identifying desoldering were derived from these tests, demonstrating that the robot had sufficient sensitivity to detect the desired variations without requiring additional force and position sensors.

A statistical analysis was conducted on tests performed with the tool to evaluate the accuracy of force data during the contact phase between the tool and the component prior to desoldering. This analysis confirmed that the system exhibited good precision and accuracy for the disassembly application. However, it was noted that the accuracy might not be sufficient if strict force values were required, necessitating the implementation of an external control circuit.

The disassembly operation was performed on PCB components attached with hot glue to a clean surface to test the system's functionality under the most uncomplicated conditions. The behavior of the data aligned with the previously observed results.

Subsequent tests aimed to evaluate the disassembly system's performance in extracting PCB components. The most significant challenges arose during the transition from the desoldering phase to the component grasping operation, both with larger PCBs (Level 2) and cell phone PCBs (Level 3). The difficulties encountered were attributable to several factors, including the presence of smaller components in the vicinity, causing the component of interest to shift during desoldering, as well as the minimal height (less than 0.5mm) that made continuous contact with the component difficult. In certain cell phone boards, components were additionally secured with resin, making desoldering impractical. However, the proposed method successfully completed the disassembly process on two PCBs (Levels 2 and 3), demonstrating the viability of the disassembly application put forth in the study. All the performed tests succeeded in the desoldering phase in almost 100%.

Throughout the work, setbacks were primarily associated with system integration issues and characteristics related to the component and PCB architecture. Integration challenges included difficulties in reading values from the robot, intermittent gripper stops that disrupted tests and necessitated restarts, and initial errors associated with publishing thermal camera data in the intended topic. The availability of only one robot meeting the required specifications for the experimental setup limited process automation, as the hot air application part had to be carried out manually. Additionally, the inability to test the system with camera data as input, as it was separate from the study work, extended the duration of the tests. Manufacturing components as thin and small as required to enhance the tool's performance proved challenging with the available resources, hindering the production of additional prototypes.

In the future, to improve the implemented robotic disassembly cell, a second robot should be integrated to apply hot air and, if possible, with a gripper architecture that would allow the introduction of a thin metal tip responsible for detecting the movement of the component. Thus, the current robot would only be responsible for the gripping action, allowing the use of other tools with other operating principles, such as suction. Changing the gripper to one with greater precision and, if possible, with integrated sensors would also improve the viability of the process. Another alternative would be the development of a new gripper specifically for the disassembly operation proposed.

Introducing a vision system will be essential to automate the disassembly process further. Leveraging data from the vision system will not only facilitate component positioning (as mentioned in the methodology chapter), but also enable component identification, orientation, and geometry analysis. This information is crucial for defining the disassembly order, particularly as the project progresses and smaller and more diverse PCBs are encountered. Additionally, it will assist in determining the optimal tool opening based on component size.

Finally, another aspect to be improved is related to the experimental setup. The current setup can adapt to some sizes of plates, but for small plates, it does not allow them to be fixed. For this, it will be necessary to increase the size of the aluminum profiles that support the adjustment structure. Concerning the structure near the base of the hot plate, this will also have to be adjusted to compensate for the gap caused by the loading part of the plate, which does not allow the support to be tight to the plate, causing a certain instability.

Despite the limitations faced, it is possible to conclude that the work done resulted in significant contributions to the project "RECY SMARTE - Sustainable approaches for recycling discarded mobile phones" since it showed that it is possible to implement a robotic disassembly

process for the extraction of components, even in its initial version. Furthermore, the unforeseen introduction of the thermal camera has highlighted the potential for integrating new sensors and their viability in future research, including a detailed thermal analysis that could prove beneficial.

Bibliography

[1] A. A. Adenuga, O. D. Amos, O. D. Olajide, A. O. Eludoyin, and O. O. Idowu, "Environmental impact and health risk assessment of potentially toxic metals emanating from different anthropogenic activities related to e-wastes," *Heliyon*, vol. 8, 8 2022.

[2] B. Kopacek, "Intelligent disassembly of components from printed circuit boards to enable re-use and more efficient recovery of critical metals," *IFAC-PapersOnLine*, vol. 49, pp. 190–195, 2016.

[3] J. F. Buhl, R. Grønhøj, J. K. Jørgensen, G. Mateus, D. Pinto, J. K. Sørensen, S. Bøgh, and D. Chrysostomou, "A dual-arm collaborative robot system for the smart factories of the future," *Procedia Manufacturing*, vol. 38, pp. 333–340, 2019.

[4] S. Cazan, D. Chirita, C. Stamate, D. Irimia, A. Burlacu, and I. Doroftei, "Dismantling strategy for capacitors placed on printed circuits boards: Challenges and preliminary results," *IOP Conference Series: Materials Science and Engineering*, vol. 997, 12 2020.

[5] G. Foo, S. Kara, and M. Pagnucco, "Challenges of robotic disassembly in practice," *Procedia CIRP*, vol. 105, pp. 513–518, 2022.

[6] H. Liu, J. Hai, L. Li, and F. Yin, "An efficient disassembly process generation method for large quantities of waste smartphones," *Procedia CIRP*, vol. 105, pp. 140–145, 2022.

[7] J. Li, M. Barwood, and S. Rahimifard, "A multi-criteria assessment of robotic disassembly to support recycling and recovery," *Resources, Conservation and Recycling*, vol. 140, pp. 158–165, 1 2019.

[8] A. A. Maurice, K. N. Dinh, N. M. Charpentier, A. Brambilla, and J. C. P. Gabriel, "Dismantling of printed circuit boards enabling electronic components sorting and their subsequent treatment open improved elemental sustainability opportunities," *Sustainability (Switzerland)*, vol. 13, 9 2021.

[9] G. Fantoni, M. Santochi, G. Dini, K. Tracht, B. Scholz-Reiter, J. Fleischer, T. K. Lien, G. Seliger, G. Reinhart, J. Franke, H. N. Hansen, and A. Verl, "Grasping devices and methods in automated production processes," *CIRP Annals - Manufacturing Technology*, vol. 63, pp. 679–701, 2014.

[10] C. Ning, C. S. K. Lin, D. C. W. Hui, and G. McKay, "Waste printed circuit board (pcb) recycling techniques," *Topics in Current Chemistry*, vol. 375, 4 2017.

[11] S. Grahn, B. Langbeck, K. Johansen, and B. Backman, "Potential advantages using large anthropomorphic robots in human-robot collaborative, hand guided assembly," *Procedia CIRP*, vol. 44, pp. 281–286, 2016.

[12] D. F. Andrade, J. P. Castro, J. A. Garcia, R. C. Machado, E. R. Pereira-Filho, and D. Amarasiriwardena, "Analytical and reclamation technologies for identification and recycling of

precious materials from waste computer and mobile phones," *Chemosphere*, vol. 286, 1 2022.

[13] E. Álvarez-de-los Mozos, A. Rentería-Bilbao, and F. Díaz-Martín, "WEEE recycling and circular economy assisted by collaborative robots," *Applied Sciences (Switzerland)*, vol. 10, 7 2020.

[14] B. Ghosh, M. K. Ghosh, P. Parhi, P. S. Mukherjee, and B. K. Mishra, "Waste printed circuit boards recycling: An extensive assessment of current status," *Journal of Cleaner Production*, vol. 94, pp. 5–19, 5 2015.

[15] S. Udayakumar, M. I. B. A. Razak, and S. Ismail, "Recovering valuable metals from waste printed circuit boards (wpcb): A short review," *Materials Today: Proceedings*, 1 2022.

[16] M. Kaya, "Recovery of metals and nonmetals from electronic waste by physical and chemical recycling processes," *Waste Management*, vol. 57, pp. 64–90, 11 2016.

[17] S. D'Avella, C. A. Avizzano, and P. Tripicchio, "Ros-industrial based robotic cell for industry 4.0: Eye-in-hand stereo camera and visual servoing for flexible, fast, and accurate picking and hooking in the production line," *Robotics and Computer-Integrated Manufacturing*, vol. 80, 4 2023.

[18] P. Corke, *Robotics, Vision and Control Fundamental Algorithms in MATLAB®*. Springer Tracts in Advanced Robotics Volume 73, 2013.

[19] T. Fang and Y. Ding, "A sampling-based motion planning method for active visual measurement with an industrial robot," *Robotics and Computer-Integrated Manufacturing*, vol. 76, 8 2022.

[20] A. S. Farhan, A. M. Bassiouny, Y. T. Afif, A. A. Gamil, M. A. Alsheikh, A. M. Kamal, K. S. Elenany, M. A. Bahour, M. I. Awad, and S. A. Maged, "Autonomous non-destructive assembly/disassembly of electronic components using a robotic arm," *Proceedings - 2021 16th International Conference on Computer Engineering and Systems, ICCES 2021*, 2021.

[21] T. Szkodny and A. Legowski, "Planning trajectories of adept six-300 robot with using of vision information," pp. 1–6, 2017.

[22] C. Cai, E. Dean-León, N. Somani, and A. Knoll, "6d image-based visual servoing for robot manipulators with uncalibrated stereo cameras," 2014.

[23] X. He, H. Luo, Y. Feng, X. Wu, and Y. Diao, "An uncalibrated image-based visual servo strategy for robust navigation in autonomous intravitreal injection," *Electronics (Switzerland)*, vol. 11, 12 2022.

[24] J. Lin, Y. Wang, Z. Miao, H. Wang, and R. Fierro, "Robust image-based landing control of a quadrotor on an unpredictable moving vehicle using circle features," *IEEE Transactions on Automation Science and Engineering*, 4 2022.

[25] R. Tedrake, *Robotic Manipulation*. Massachusetts Institute of Technology (MIT), 2022.

[26] P. Corke, *Robotics, Vision and Control Fundamental Algorithms in MATLAB®*. Springer Tracts in Advanced Robotics Volume 73, 2013.

[27] Z. Wang, H. Li, and X. Zhang, "Construction waste recycling robot for nails and screws: Computer vision technology and neural network approach," *Automation in Construction*, vol. 97, pp. 220–228, 1 2019.

[28] J. P. J. Prioli, H. M. Alrufaifi, and J. L. Rickli, "Disassembly assessment from cad-based collision evaluation for sequence planning," *Robotics and Computer-Integrated Manufacturing*, vol. 78, 12 2022.

[29] F. Ye, J. Perrett, L. Zhang, Y. Laili, and Y. Wang, "A self-evolving system for robotic disassembly sequence planning under uncertain interference conditions," *Robotics and Computer-Integrated Manufacturing*, vol. 78, 12 2022.

[30] J. N. Pires and T. Godinho, "Controlo de força em robótica industrial," *Revista Iberoamericana de Ingeniería Mecánica*, vol. 10, pp. 2–13, 2006.

[31] A. Calanca, R. Muradore, and P. Fiorini, "A review of algorithms for compliant control of stiff and fixed-compliance robots," *IEEE/ASME Transactions on Mechatronics*, vol. 21, pp. 613–624, 4 2016.

[32] W. Kraus, P. Miermeister, V. Schmidt, and A. Pott, "Hybrid position-force control of a cable-driven parallel robot with experimental evaluation," *Mechanical Sciences*, vol. 6, pp. 119–125, 8 2015.

[33] O. Khatib and J. Burdick, "Motion and force control of robot manipulators.," pp. 1381–1386, 1986.

[34] X. Xu, W. Chen, D. Zhu, S. Yan, and H. Ding, "Hybrid active/passive force control strategy for grinding marks suppression and profile accuracy enhancement in robotic belt grinding of turbine blade," *Robotics and Computer-Integrated Manufacturing*, vol. 67, 2 2021.

[35] J. Huang, D. T. Pham, Y. Wang, C. Ji, W. Xu, Q. Liu, and Z. Zhou, "A strategy for human-robot collaboration in taking products apart for remanufacture," *FME Transactions*, vol. 47, pp. 731–738, 2019.

[36] A. S. Sadun, J. Jalani, and J. A. Sukor, "An overview of active compliance control for a robotic hand," vol. 11, 2016.

[37] F. Chen, H. Zhao, D. Li, L. Chen, C. Tan, and H. Ding, "Contact force control and vibration suppression in robotic polishing with a smart end effector," *Robotics and Computer-Integrated Manufacturing*, vol. 57, pp. 391–403, 6 2019.

[38] K. Song, G. Xiao, S. Chen, X. Liu, and Y. Huang, "A new force-depth model for robotic abrasive belt grinding and confirmation by grinding of the inconel 718 alloy," *Robotics and Computer-Integrated Manufacturing*, vol. 80, p. 102483, 4 2023.

[39] W. Zhang, H. Cheng, L. Hao, X. Li, M. Liu, and X. Gao, "An obstacle avoidance algorithm for robot manipulators based on decision-making force," *Robotics and Computer-Integrated Manufacturing*, vol. 71, 10 2021.

[40] M. Amersdorfer, J. Kappey, and T. Meurer, "Real-time freeform surface and path tracking for force controlled robotic tooling applications," *Robotics and Computer-Integrated Manufacturing*, vol. 65, 10 2020.

[41] D. Jinjun, G. Yahui, C. Ming, and D. Xianzhong, "Symmetrical adaptive variable admittance control for position/force tracking of dual-arm cooperative manipulators with unknown trajectory deviations," *Robotics and Computer-Integrated Manufacturing*, vol. 57, pp. 357–369, 6 2019.

[42] X. Sun, C. Wang, W. Chen, W. Chen, G. Yang, and Y. Jin, "A single-actuator four-

finger adaptive gripper for robotic assembly," *IEEE Transactions on Industrial Electronics*, pp. 1–10, 1 2023.

[43] S. Su, D. T. Pham, C. Ji, Y. Wang, J. Huang, W. Zhou, and H. Wang, "Design of a compliant device for peg-hole separation in robotic disassembly," *International Journal of Advanced Manufacturing Technology*, vol. 124, pp. 3011–3019, 2 2023.

[44] P. V. K. Rao, M. V. Subramanyam, and K. Satyaprasad, "Study on pid controller design and performance based on tuning techniques," *2014 International Conference on Control, Instrumentation, Communication and Computational Technologies, ICCICCT 2014*, pp. 1411–1417, 12 2014.

[45] R. Pérez-Ubeda, R. Zotovic-Stanisic, and S. C. Gutiérrez, "Force control improvement in collaborative robots through theory analysis and experimental endorsement," *Applied Sciences*, vol. 10, no. 12, 2020.

[46] P. Neranon and R. Bicker, "Force/position control of robot manipulator for human-robot interaction," *Thermal Science*, vol. 20, pp. 36–36, 01 2016.

[47] P. Sanchez-Sanchez and F. Reyes-Cortes, *Cartesian Control for Robot Manipulators*. In-Tech, 3 2010.

[48] Z. Fan, K. Jia, L. Zhang, F. Zou, Z. Du, M. Liu, Y. Cao, and Q. Zhang, "A cartesian-based trajectory optimization with jerk constraints for a robot," *Entropy*, vol. 25, 4 2023.

[49] D. Prattichizzo and J. C. Trinkle, *Grasping*, pp. 955–988. Cham: Springer International Publishing, 2016.

[50] G. Fantoni, M. Santochi, G. Dini, K. Tracht, B. Scholz-Reiter, J. Fleischer, T. K. Lien, G. Seliger, G. Reinhart, J. Franke, H. N. Hansen, and A. Verl, "Grasping devices and methods in automated production processes," *CIRP Annals - Manufacturing Technology*, vol. 63, pp. 679–701, 2014.

[51] W. H. Chen, G. Foo, S. Kara, and M. Pagnucco, "Application of a multi-head tool for robotic disassembly," *Procedia CIRP*, vol. 90, pp. 630–635, 2020. 27th CIRP Life Cycle Engineering Conference (LCE2020) Advancing Life Cycle Engineering : from technological eco-efficiency to technology that supports a world that meets the development goals and the absolute sustainability.

[52] A. Cloutier and J. Yang, "Grasping force optimization approaches for anthropomorphic hands," *Journal of Mechanisms and Robotics*, vol. 10, 2 2018.

[53] S. Ruggeri, G. Fontana, V. Basile, M. Valori, and I. Fassi, "Micro-robotic handling solutions for pcb (re-)manufacturing," *Procedia Manufacturing*, vol. 11, pp. 441–448, 2017. 27th International Conference on Flexible Automation and Intelligent Manufacturing, FAIM2017, 27-30 June 2017, Modena, Italy.

[54] B. Zhang, Y. Xie, J. Zhou, K. Wang, and Z. Zhang, "State-of-the-art robotic grippers, grasping and control strategies, as well as their applications in agricultural robots: A review," *Computers and Electronics in Agriculture*, vol. 177, 10 2020.

[55] C. Klas, F. Hundhausen, J. Gao, C. R. G. Dreher, S. Reither, Y. Zhou, and T. Asfour, "The kit gripper: A multi-functional gripper for disassembly tasks," in *2021 IEEE International Conference on Robotics and Automation (ICRA)*, pp. 715–721, 2021.

[56] K. Naito, A. Shirai, S. I. Kaneko, and G. Capi, "Recycling of printed circuit boards by

robot manipulator: A deep learning approach," *IEEE International Symposium on Robotic and Sensors Environments, ROSE 2021 - Proceedings*, 2021.

[57] M. Kaya, *Dismantling and Desoldering*, pp. 69–82. Cham: Springer International Publishing, 2019.

[58] I. Doroftei and A. Burlacu, "Eye-to-hand architecture for pcb automated dismantling procedures," *2020 23rd IEEE International Symposium on Measurement and Control in Robotics, ISMCR 2020*, 10 2020.

[59] S. Cazan, D. Chirita, C. Stamate, D. Irimia, A. Burlacu, and I. Doroftei, "Dismantling strategy for capacitors placed on printed circuits boards: challenges and preliminary results," *IOP Conference Series Materials Science and Engineering*, vol. 997, p. 012071, 12 2020.

[60] R. Noll, R. Ambrosch, K. Bergmann, S. Britten, H. Brumm, A. Chmielarz, S. Connemann, M. Eschen, A. Frank, C. Fricke-Begemann, C. Gehlen, T. Gorewoda, M. Guolo, W. Kurylak, J. Makowe, G. Sellin, M. Siguier, A. Tori, and F. Veglia, "Next generation urban mining-automated disassembly, separation and recovery of valuable materials from elec-tronic equipment: overview of rd approaches and first results of the european project adir," 2017.

[61] C. He, Z. Jin, R. Gu, and H. Qu, "Automatic disassembly and recovery device for mobile phone circuit board cpu based on machine vision," *Journal of Physics: Conference Series*, vol. 1684, p. 012137, nov 2020.

[62] J. Li, M. Barwood, and S. Rahimifard, "Robotic disassembly for increased recovery of strategically important materials from electrical vehicles," *Robotics and Computer-Integrated Manufacturing*, vol. 50, pp. 203–212, 4 2018.

[63] J. Li, X. Zhang, and P. Feng, "Detection method of end-of-life mobile phone components based on image processing," *Sustainability (Switzerland)*, vol. 14, 10 2022.

[64] W. H. Chen, G. Foo, S. Kara, and M. Pagnucco, "Automated generation and execution of disassembly actions," *Robotics and Computer-Integrated Manufacturing*, vol. 68, 4 2021.

[65] J. Huang, D. T. Pham, R. Li, M. Qu, Y. Wang, M. Kerin, S. Su, C. Ji, O. Mahomed, R. Khalil, D. Stockton, W. Xu, Q. Liu, and Z. Zhou, "An experimental human-robot collaborative disassembly cell," *Computers and Industrial Engineering*, vol. 155, 5 2021.

[66] M. L. Lee, S. Behdad, X. Liang, and M. Zheng, "Task allocation and planning for product disassembly with human–robot collaboration," *Robotics and Computer-Integrated Manufacturing*, vol. 76, 8 2022.

[67] D. R. Inc., *Reference manual*. Doosan Robotics Inc., 2022.

[68] M. Spong, S. Hutchinson, and M. Vidyasagar, *Robot Modeling and Control*. Wiley, 2005.

[69] J. Park, "The relationship between controlled joint torque and end-effector force in underactuated robotic systems," *Robotica*, vol. 29, no. 4, p. 581–584, 2011.

[70] D. R. Inc., *User manual*. Doosan Robotics Inc., 2022.

[71] B. Siciliano, L. Sciavicco, V. Luigi, and G. Oriolo, *Robotics: Modelling, Planning and Control*. 01 2011.

[72] R. Pérez-Ubeda, R. Zotovic-Stanisic, and S. C. Gutiérrez, "Force control improvement

in collaborative robots through theory analysis and experimental endorsement," *Applied Sciences*, vol. 10, no. 12, 2020.